

Optimal Regulation of Blood Glucose Level in Type I Diabetes using Insulin and Glucagon

Afroza Shirin*, Fabio Della Rossa, Isaac S. Klickstein, John J. Russell, Francesco Sorrentino

Mechanical Engineering Department, University of New Mexico, Albuquerque, NM 87131

* ashirin@unm.edu

Abstract

The Glucose-Insulin-Glucagon nonlinear model [1–4] accurately describes how the body responds to exogenously supplied insulin and glucagon in patients affected by Type I diabetes. Based on this model, we design infusion rates of either insulin (monotherapy) or insulin and glucagon (dual therapy) that can optimally maintain the blood glucose level within desired limits after consumption of a meal and prevent the onset of both hypoglycemia and hyperglycemia. This problem is formulated as a nonlinear optimal control problem, which we solve using the numerical optimal control package *PSOPT*. Interestingly, in the case of monotherapy, we find the optimal solution is close to the standard method of insulin based glucose regulation, which is to assume a variable amount of insulin half an hour before each meal. We also find that the optimal dual therapy (that uses both insulin and glucagon) is better able to regulate glucose as compared to using insulin alone. We also propose an *ad-hoc* rule for both the dosage and the time of delivery of insulin and glucagon.

1 Introduction

Insulin and glucagon are pancreatic hormones that help regulate the levels of glucose in the blood. Insulin is produced by the *beta-cells* in the pancreas and carries glucose from the bloodstream to the cells throughout the body. Glucagon releases glucose from the liver into the bloodstream in order to prevent hypoglycemia. In people affected by diabetes insulin is either absent (type I diabetes) or not produced in the proper amount (type II diabetes). In type I diabetes the body's immune system attacks and destroys the beta cells. As a result, insulin is not produced and glucose accumulates in the blood which may cause serious harm to several organs. Type II diabetes is a metabolic disorder in which the beta cells are unable to properly regulate the blood glucose within limits. Common therapies for diabetes involve the administration of exogenous insulin. Currently glucagon is not typically included in therapies because it does not preserve its chemical properties at room temperature and also because diabetic patients are still able to produce it.

The control of glucose levels in diabetic patients is an active field of research [5–19]. The approval by the FDA of a simulator which replaces *in-vivo* with *in-silico* therapy testing has greatly benefited this area of research. This simulator implements a mathematical model, first proposed in [1] and updated in [2–4], and provides an alternative to often slow, dangerous and expensive human testing.

Typically, insulin is administered manually approximately half an hour before each meal where the amount is determined from the current glucose level (measured through a blood sugar test), the expected glucose intake, and the patient's sensitivity to insulin. In what follows we will refer to this as the *standard therapy*. In 1992 the first insulin pumps were introduced to the

market. They delivered both a consistent basal amount of insulin and an insulin bolus determined by the patients based on their glucose level. It was only in 2016 that the first autonomous system for glycemic control was approved by the FDA. The system consists of an insulin pump, a sensor that measures the blood glucose level continuously in time, and control software that is able to regulate the insulin level in the blood without needing any input from the patient.

Many control techniques have been proposed and tested to regulate blood glucose levels using insulin pumps including PID (proportional–integral–derivative) control [5, 6, 8–10, 20], fuzzy logic control [11–13] and bio-inspired techniques [14] which do not rely on a mathematical model. In [21] closed loop control has been used on a so called “minimal model” [22–24]. In [15–18, 25] a linear model predictive control (MPC) has been used in a model with fixed structure but for which parameters are constantly updated to adapt to the patient’s response. In [26] linear MPC has been used *in silico*. In [27] MPC has been applied to a system linearized around the operating points of a physically derived nonlinear model and in [28] multiple model probabilistic predictive control has been used. In [29] MPC has been applied together with a moving horizon estimation technique to a linear model. Most of the models used when designing the above controllers are simplified versions of the FDA approved model and all the control techniques considered only use insulin (but not glucagon) as control input.

Because insulin delivered exogenously is not subject to normal physiological feedback regulation, hypoglycemia is common in patients with Type 1 diabetes who undergo treatment [30]. For these patients it has been proposed that exogenous insulin can be used to lower their blood glucose level and exogenous glucagon can be used to prevent hypoglycemia [31, 32]. Currently, a commercial pump that delivers both insulin and glucagon is not available, and the development of a two-drug artificial pancreas is still the subject of clinical research [33–41]. An outstanding research question, which we address in this paper, is the determination of the temporal dosages of both insulin and glucagon, in the case of the dual therapy.

Following the study in [42] which optimized multi-drug therapies for autophagy regulation, here we seek to determine an optimal strategy for delivery of both insulin and glucagon. We consider the combined effects of insulin and glucagon in regulating blood glucose levels in patients with Type 1 diabetes, using the model in [3] and nonlinear optimal control theory. Additionally, the objective function that we seek to minimize is the Blood Glucose Index which is a well known tool to measure the risk for a patient to enter either hyperglycemia or hypoglycemia. To design the optimal control problem, we use the balance control technique of ref. [43], which introduces a trade-off between the error allowed with respect to a state based cost (Blood Glucose Index) and the control effort. Our goal is to evaluate the performance limits of a control algorithm in the blood glucose problem, and to discuss the advantages of the dual drug therapy compared to the single drug therapy. Note that even though we do not attempt to design a closed-loop control strategy that works without the patient’s intervention, the solution we propose can be adapted for that purpose.

From solving the optimal control problem for a family of objective functions derived from the balance control paradigm, we observe the emergence of a pattern, from which we propose a simple rule for the delivery of insulin and glucagon similar to the standard therapy, but for the case that both insulin and glucagon are used. While this therapy is suboptimal, we see that it still performs better than the optimal solution with insulin alone.

Finally, we test the robustness of the optimal solution. While optimal control does not guarantee robustness of the optimal solution with respect to model uncertainty or parameter mismatches, we see that our proposed solution still performs well in the presence of model parameter perturbations and variations affecting the time and glucose intake of the meal.

2 Materials and methods

2.1 Model and Parameters

We consider the model in [3, 4] which is a system of nonlinear ordinary differential equations (ODEs). The equations are given in Eqs. (S1)–(S9) in supplementary information section S1. We write the ODEs in Eqs. (S1)–(S9) in the form

$$\begin{aligned}\dot{\mathbf{x}}(t) &= \mathbf{f}(\mathbf{x}(t), \mathbf{u}(t), D(t), \Theta) \\ G(t) &= x_1/V_G\end{aligned}\quad (1)$$

where the state vector is $\mathbf{x} = [x_1(t), x_2(t), \dots, x_{17}(t)]^T$ and t is the physical time (in min). In Table 1 we tabulate all of the variables x_i and their names. The control input vector is $\mathbf{u}(t) = [u_I(t), u_G(t)]^T$, where $u_I(t) \geq 0$ is the exogenous insulin infusion rate (in insulin Unit/min) and $u_G(t) \geq 0$ is the exogenous glucagon infusion rate (mg/min). Both $u_I(t)$ and $u_G(t)$ are the external inputs to the system in Eq. (1). The scalar quantity $D(t)$ represents the exogenous glucose input, that is, the glucose intake with a meal. The output of the system is the quantity $G(t)$, which measures the density of glucose in the blood, obtained as the ratio between the plasma glucose and the distribution volume of glucose V_G .

When $u_I(t) = 0$, $u_G(t) = 0$ and $D(t) = 0$, the model reaches (for physically meaningful parameters) a steady state, also known as the *basal condition* of a patient. The basal condition depends upon the parameters of the models Θ . We denote by Θ_{G_b} a set of parameters for which the basal glucose level G is equal to G_b . The basal levels for the other states are found according to Eqs. (S11).

Table 1. Variables and their physical meaning

Variables	Names	Representing	Units
x_1	G_p	Mass of glucose in plasma	mg/kg
x_2	G_t	Mass of glucose in tissue	mg/kg
x_3	I_l	Mass of insulin in liver	pmol/kg
x_4	I_p	Mass of insulin in plasma	pmol/kg
x_5	I'	Mass of delayed in compartment 1	pmol/L
x_6	X^L	Amount of delayed insulin action on <i>EGP</i> (Endogenous glucose production)	pmol/L
x_7	Q_{sto1}	Amount of solid glucose in stomach	mg
x_8	Q_{sto2}	Amount of liquid glucose in stomach	mg
x_9	Q_{gut}	Amount of glucose in intestine	mg
x_{10}	X	Amount of interstitial fluid	pmol/L
x_{11}	SR_H^s	Amount of static glucagon	ng/L/min
x_{12}	H	Amount plasma glucagon	ng/L
x_{13}	X^H	Amount of delayed glucagon action on <i>EGP</i>	ng/L
x_{14}	I_{sc1}	Amount of nonmonomeric insulin in the subcutaneous space	pmol/kg
x_{15}	I_{sc2}	Amount of monomeric insulin	pmol/kg
x_{16}	H_{sc1}	Amount of glucagon in the subcutaneous space 1	ng/L
x_{17}	H_{sc2}	Amount of glucagon in the subcutaneous space 2	ng/L

State variables and their physical meaning.

2.2 Problem Formulation

We formulate a nonlinear optimal control problem with two control goals. The first goal is to regulate the glucose at levels corresponding to low clinical risk of either hyperglycemia or

hypoglycemia during a time period over which a meal is consumed. We assume that a meal is ingested at time $t = \tau_D$, which we assume to be modeled as a Dirac delta function $D(t) = D\delta(t - \tau_D)$. To evaluate the clinical risk of a particular glycemc value, Kovatchev et al. [44, 45] proposed the *Blood Glucose Index* (BGI), defined as

$$BGI(G(t)) = 10 \left(1.509 \left((\ln G(t))^{1.084} - 5.3811 \right) \right)^2,$$

where a small BGI value corresponds to low risk of either hyperglycemia or hypoglycemia. This metric also takes into account the fact that (i) the target blood glucose range as defined by the Diabetes Control and Complications Trial [46] (between 70 and 180 mg/dL) is not symmetric about the center of the range and (ii) hypoglycemia occurs at glucose levels closer to the basal level than hyperglycemia. The second goal is to limit the overall usage of insulin and/or glucagon over the period $[t_0, t_f]$.

We formulate the optimization problem according to these two goals,

$$\min_{\mathbf{u}(t)} J = \int_{t_0}^{t_f} [\alpha_p BGI(G(t)) + \alpha_I u_I^p(t) + \alpha_G u_G^p(t)] dt, \quad (2)$$

subject to the following constraints,

$$\dot{\mathbf{x}}(t) = \mathbf{f}(\mathbf{x}(t), \mathbf{u}(t), D\delta(t - \tau_D), \Theta_{G_b}), \quad \mathbf{u}(t) = [u_I(t) \quad u_G(t)]^T \quad (3a)$$

$$G^L < G(t) < G^U \quad (3b)$$

$$u_I^L \leq u_I(t) \leq u_I^U \quad (3c)$$

$$0 \leq u_G(t) \leq u_G^U \quad (3d)$$

$$0 \leq \int_{t_0}^{t_f} u_I(t) dt \leq \phi_I^U \quad (3e)$$

$$0 \leq \int_{t_0}^{t_f} u_G(t) dt \leq \phi_G^U \quad (3f)$$

$$\mathbf{x}(t_0) = \bar{\mathbf{x}} \quad (3g)$$

In Eqs. (2) and (3), the insulin infusion rate $u_I(t)$ and the glucagon infusion rate $u_G(t)$ are the two control inputs. The three coefficients α_p , α_I and α_G in Eq. (2) are tunable factors through which we may vary the weight associated with each of the three terms in the cost function J . The first coefficient, α_p is dimensionless while the units of α_I and α_G are $(\text{U}/\text{min})^{-p}$ and $(\text{mg}/\text{min})^{-p}$, respectively. Note that by setting $u_G = 0$ in Eq. (3d), we have an optimal control problem in terms of insulin only.

The first term in the objective function (2) defines a regulation problem, *i.e.*, we try to maintain the glucose at low risk levels. The second and third terms in the cost function are chosen to avoid using excess insulin or glucagon. For $p = 1$ in Eq. (2), the second and third terms define a ‘*minimum fuel*’ problem, thus we call the optimization problem ReMF (Regulation and Minimum Fuel). In this case, we expect the optimal solution to consist of pulsatile inputs $u_I^*(t)$ and $u_G^*(t)$ [47, 48]. For $p = 2$, the second and third term inside the cost function define a ‘*minimum energy*’ problem, thus we call the optimization problem ReME (Regulation and Minimum Energy). In this case, we expect the optimal control inputs $u_I^*(t)$ and $u_G^*(t)$ to be continuous. The set of equations in (3a) coincide with the ODEs in Eqs. (S1)-(S9) of the supplemental information. In Eq. (3b) G^L and G^U are the lower and upper bounds for $G(t)$, they can be set in order to avoid undesired hypoglycemic or hyperglycemic states. In Eqs. (3c) and (3d) u_I^U and u_G^U are upper bounds for the insulin and glucagon delivery rates, respectively. These constraints are set by the maximum infusion rates allowed by the insulin pump. In Eq. (3c) $u_I^L \geq 0$ is the lower bound for $u_I(t)$, *i.e.*, a minimum insulin delivery rate that can be used to set a basal insulin infusion rate to counteract endogenous glucose production [49]. Finally, in Eqs. (3e, 3f), ϕ_I^U and ϕ_G^U set limits to the total limits of insulin and glucagon that can be delivered

over the time period $[t_0, t_f]$. The initial condition $\bar{\mathbf{x}}$ in Eq. (3g) defines the patient's condition before administration of the therapy. In the Results section, we discuss how we choose the bounds on $G(t)$, $u_I(t)$, $u_G(t)$, ϕ_I , ϕ_G , the control time period $[t_0, t_f]$ and the initial condition $\bar{\mathbf{x}}$.

Our goal is to find an optimal solution which satisfies the constraints in Eq. (3) and minimizes the objective function (2). Note that the BGI only depends upon $G(t)$: we are making no attempt to control the states of the system, only its output. In the literature, such an approach is often referred to as target control [47, 50].

2.3 Method: Pseudo-Spectral Optimal Control

Optimal control theory combines aspects of dynamical systems, optimization, and the calculus of variations [47] to solve the problem of finding a control law for a given dynamical system such that the prescribed optimality criteria are achieved. The equations (2) and (3) together form a constrained optimal control problem, which can generally be written as,

$$\begin{aligned} \min_{\mathbf{u}(t)} \quad & J(\mathbf{x}(t), \mathbf{u}(t), t) = \int_{t_0}^{t_f} F(\mathbf{x}(t), \mathbf{u}(t), t) dt \\ \text{s.t.} \quad & \dot{\mathbf{x}}(t) = \mathbf{f}(\mathbf{x}(t), \mathbf{u}(t), t) \\ & \mathbf{e}^L \leq \mathbf{e}(\mathbf{x}(t_0), \mathbf{x}(t_f), t_0, t_f) \leq \mathbf{e}^U \\ & \mathbf{h}^L \leq \mathbf{h}(\mathbf{x}(t), \mathbf{u}(t), t) \leq \mathbf{h}^U \\ & t \in [t_0, t_f] \end{aligned} \quad (4)$$

In general, there exists no analytic framework that is able to provide the optimal time traces of the controls $\mathbf{u}^*(t)$ and the states $\mathbf{x}^*(t)$ in (4), and so we must resort to numerical techniques.

Pseudo-Spectral Optimal Control (PSOC) is a computational method for solving optimal control problems. Here we present a brief overview of the theory of pseudo-spectral optimal control. PSOC has become a popular tool in recent years [51, 52] that has let scientists and engineers solve optimal control problems like (4) reliably and efficiently in applications such as guiding autonomous vehicles and maneuvering the international space station [52]. PSOC is an approach by which an OCP can be discretized by approximating the integrals by quadratures and the time-varying states and control inputs with interpolating polynomials. Here we summarize the main concept of the PSOC. We choose a set of N discrete times $\{\tau_i\}$ $i = 0, 1, \dots, N$ where $\tau_0 = -1$ and $\tau_N = 1$ with a mapping between $t \in [t_0, t_f]$ and $\tau \in [-1, 1]$. The times $\{\tau_i\}$ are chosen as the roots of an $(N + 1)$ th order orthogonal polynomial such as Legendre polynomials or Chebyshev polynomials. The choice of discretization scheme is important to the convergence of the full discretized problem. For instance, if we choose the roots of a Legendre polynomial as the discretization scheme, the associated quadrature weights can be found in the typical way for Gauss quadrature. The time-varying states and control inputs are found by approximating them with Lagrange interpolating polynomials,

$$\hat{\mathbf{x}}(\tau) = \sum_{i=0}^N \hat{\mathbf{x}}_i L_i(\tau) \quad (5a)$$

$$\hat{\mathbf{u}}(\tau) = \sum_{i=0}^N \hat{\mathbf{u}}_i L_i(\tau), \quad (5b)$$

where $\hat{\mathbf{x}}(\tau)$ and $\hat{\mathbf{u}}(\tau)$ are the approximations of $\mathbf{x}(\tau)$ and $\mathbf{u}(\tau)$, respectively, and $L_i(\tau)$ is the i th Lagrange interpolating polynomial. The dynamical system is approximated by differentiating the approximation $\hat{\mathbf{x}}(\tau) = \sum_{i=0}^N \hat{\mathbf{x}}_i L_i(\tau)$ with respect to time.

$$\frac{d\hat{\mathbf{x}}}{d\tau} = \sum_{i=0}^N \hat{\mathbf{x}}_i \frac{dL_i}{d\tau} \quad (6)$$

Let $D_{k,i} = \frac{d}{d\tau} L_i(\tau_k)$ which allows one to rewrite the original dynamical system constraints in (4) as the following set of algebraic constraints.

$$\sum_{i=0}^N D_{k,i} \mathbf{x}_i - \frac{t_f - t_0}{2} \mathbf{f}(\hat{\mathbf{x}}_i, \hat{\mathbf{u}}_i, \tau_i) = \mathbf{0}, \quad k = 1, \dots, N \quad (7)$$

The integral in the cost function is approximated as,

$$J = \int_{t_0}^{t_f} F(\mathbf{x}, \mathbf{u}, t) \approx \hat{J} = \frac{t_f - t_0}{2} \sum_{k=1}^N F(\hat{\mathbf{x}}_k, \hat{\mathbf{u}}_k, \tau_k) \quad (8)$$

The original time-varying states, control inputs, the dynamical equations constrained and the cost function are now discretized approximation of the continuous NLP problem. Thus the discretized approximation of the original OCP is compiled into the following nonlinear programming (NLP) problem.

$$\begin{aligned} \min_{\substack{\mathbf{u}_i \\ i=0, \dots, N}} \quad & \hat{J} = \frac{t_f - t_0}{2} \sum_{i=0}^N w_i f(\hat{\mathbf{x}}_i, \hat{\mathbf{u}}_i, \tau_i) \\ \text{s.t.} \quad & \sum_{i=0}^N D_{k,i} \hat{\mathbf{x}}_i - \frac{t_f - t_0}{2} \mathbf{f}(\hat{\mathbf{x}}_k, \hat{\mathbf{u}}_k, \tau_k) = \mathbf{0}, \quad k = 0, \dots, N \\ & \mathbf{e}^L \leq \mathbf{e}(\hat{\mathbf{x}}_0, \hat{\mathbf{x}}_N, \tau_0, \tau_N) \leq \mathbf{e}^U \\ & \mathbf{h}^L \leq \mathbf{h}(\hat{\mathbf{x}}_k, \hat{\mathbf{u}}_k, \tau_k) \leq \mathbf{h}^U, \quad k = 0, \dots, N \\ & t_i = \frac{t_f - t_0}{2} \tau_i + \frac{t_f + t_0}{2} \end{aligned} \quad (9)$$

We have used *PSOPT* [53], an open-source PSOC library, to perform the above PSOC discretization procedure. The NLP in (9) can be solved with a number of different techniques, but here we use an interior point algorithm [54] as implemented in the open-source software Ipopt [55].

2.3.1 Continuous Approximation of Non-differential Function in ODEs

The optimization algorithms implemented in *PSOPT* require the derivatives of the function $\mathbf{f}(\mathbf{x}(t), \mathbf{u}(t), \Theta_{G_b})$ exists. As there are terms that contain discontinuities in Eqs. (S1)-(S9), we replace them with smooth approximations which are described in section S3 of the SI.

3 Results

We now describe in more detail the optimal control problem in Eqs. 2 and 3 by setting the constraint and parameter values. In Fig. 1A we plot the function $BGI(G)$ versus the glucose G . The minimum $BGI(G)$ occurs at $G = G_d = 112.51$ mg/dL, which corresponds to a clinical target set for the glucose level [46]. Based on the data in [56], the average fasting plasma glucose level of patients with type I diabetes is $G_b = 130$ (mg/dL). Thus, we set the the basal glucose level $G_b = 130$ (mg/dL). The parameters Θ_{G_b} are set so that the steady state glucose is 130 (mg/dL) in the absence of a meal and of exogenously supplied insulin, *i.e.*, we compute Θ_{130} .

We set the upper and lower bounds for the glucose level, G^L and G^U in Eq. (3b), to satisfy the target blood glucose range, $90 \leq G(t) \leq 180$ [46]. The control time period is $[t_0, t_f] = [0, 300]$ minutes, and we assume that a meal with 70 grams of glucose is consumed at time $t = 60$ min (*i.e.*, $D(t) = 70\delta(t - 60)$).

We consider a situation in which the patient's glucose level is partially controlled by providing a constant but low insulin infusion rate $u_b > 0$ (which is common for patients who use

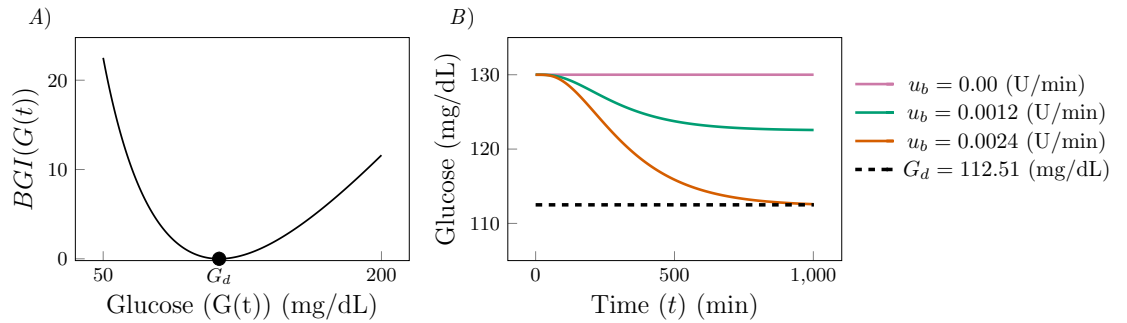


Fig 1. A) The Blood Glucose Index ($BGI(G(t))$) as a function of the blood glucose $G(t)$. The function is minimized at $G(t) = G_d = 112.51$ (mg/dL). B) The response of glucose ($G(t)$) to different time-constant basal insulin infusion rates in the absence of a meal. We see that as u_b increases, the glucose is further down regulated.

an insulin pump) [49] and serves to compensate for the endogenous glucose production. In figure 1B we show glucose response $G(t)$ for different values of constant u_b in the absence of a meal. We observe that for $u_b = 0.0024$ (U/min), $G(t)$ converges to the desired glucose level G_d . We thus set the lower bound of $u_I(t)$ in Eq. (3c), $u_I^L = u_b$, while its upper bound is set to $u_I^U = 15$ (in U/min), the maximum insulin flow allowed in commercial pumps [57]. In the absence of commercially available glucagon pumps, we will assume that a pump mechanically similar to an insulin pump is used to deliver glucagon. Since the maximum flow rate for an insulin pump is 0.15 mL/min (1 mL of insulin solution contains 100 U of insulin), and normally 1 mg of glucagon is diluted in 1 mL of solution, the maximum glucagon flow rate in Eq. (3d) is set to $u_G^U = 0.15$ mg/min.

The amount of insulin administered in a bolus to a patient with a basal glucose level lower than 150 mg/dL normally ranges between 0.12 and 0.2 U/kg [58]. As the body mass of the *in-silico* patient we consider is 78 kg, we set $\phi_I^U = 16$ U in Eq. (3e). The maximum total amount of glucagon administered in one shot to a patient who is in a hypoglycemic state is 1 mg, and a second identical shot can be administered after thirty minutes. We thus choose the maximum total amount of glucagon used (as defined in Eq. (3f)) throughout the five hour therapy to be $\phi_G^U = 1$ mg.

The choice of the initial condition \bar{x} in Eq. (3g) is critical. We select the initial condition so that the solution of our optimal control problem only attempts to regulate glucose in response to a meal. In the results presented we have set the initial condition equal to the values of the states when $u_I(t) = u_b$ after a period of fasting (the final point of the blue curve in Fig. 1B). If we were to select any alternative initial condition then the solution to the optimal control problem would try to ‘correct’ the initial condition as well, making comparisons between solutions difficult.

Once the parameters, bounds, the control time period and the initial condition are set, we solve the nonlinear optimal control problem using *PSOPT*. We first solve the optimal control problem without glucagon (*i.e.*, $u_G^U = 0$), and then we solve the optimal control problem using both insulin and glucagon.

To evaluate the effectiveness of the obtained results, we introduce the following measures.

- The cumulative insulin $r_I(t)$ and cumulative glucagon $r_G(t)$ used up to time t ,

$$r_I(t) = \int_{t_0}^t u_I(\tau) d\tau, \quad r_G(t) = \int_{t_0}^t u_G(\tau) d\tau.$$

- The total amount of insulin $\phi_I = r_I(t_f)$ and the total amount of glucagon $\phi_G = r_G(t_f)$ used up to final time t_f .

- The integral of BGI over the entire time period $[t_0, t_f]$,

$$\Delta = \int_{t_0}^{t_f} BGI(G(t))dt.$$

where a large Δ indicates that the patient is at higher risk of either hyperglycemia or hypoglycemia for a prolonged period of time.

- The maximum and minimum values attained by the blood glucose level over the entire time period $[t_0, t_f]$,

$$G^{\max} = \max_{t \in [t_0, t_f]} G(t), \quad G^{\min} = \min_{t \in [t_0, t_f]} G(t),$$

which measure the risk for either hyperglycemia or an hypoglycemia [45, 59], respectively.

3.1 Insulin as Control Input

In this section we use only insulin as control input, *i.e.*, we set $u_G = 0$ in Eq. (3a). As the orders of magnitude of the terms BGI and u_I^p in the objective function are different, it is important to find the appropriate values of the scaling factors α_p and α_I . In what follows, we use a *Pareto-front* analysis to determine these values. We first rewrite the objective function as

$$J = \int_{t_0}^{t_f} [\varepsilon BGI(G(t)) + u_I^p] dt \quad (10)$$

where $\varepsilon = \alpha_p/\alpha_I$. In Figs. 2(A–D) we plot Δ , G^{\min} , G^{\max} and ϕ_I as functions of the coefficient ε . By looking at these plots, we see that the four measures can be divided into two groups. On the one hand, Δ and G^{\max} (panels A and C), improve (decrease) as ε increases, with a sharp transition around $\varepsilon = 10$ for the ReMF problem and around $\varepsilon = 10^3$ for the ReME problem. On the other hand, G^{\min} and ϕ_I (panels B and D), behave in the opposite way, *i.e.*, they improve (insulin decreases and the minimum glucose level increases) as ε decreases, again with a sharp transition around $\varepsilon = 10$ for the ReMF problem and around $\varepsilon = 10^3$ for the ReME problem. Because the four curves in Figs. 2(A–D) are monotone, all the points are Pareto-efficient, *i.e.*, it is not possible to improve one objective (*e.g.*, Δ) without worsening the other one (*e.g.*, ϕ_I). We notice that past a certain value of ε (10 in the ReMF case, 10^3 in the ReME case) Δ and G^{\max} do not further decrease and G^{\min} and ϕ_I remain unchanged. We choose as weights $\alpha_p = 10$ and $\alpha_I = 1$ for $p = 1$, while we choose $\alpha_p = 10^3$ and $\alpha_I = 1$ for $p = 2$ (these are highlighted by dashed circles in Fig. 2). The reason for these choices (for both values of p) is that these values yield $\phi_I \sim 10$ units, which is equal to two thirds of the maximum amount of insulin that can be supplied (ϕ_I^U), and $G^{\min} \sim 93\text{mg/dL}$, which is far from the hypoglycemic risk region.

In Fig. 2E, we plot a projection of the Pareto front in the Δ and ϕ_I plane. Looking at this plot, the trade-off between Δ and ϕ_I is evident; if the total amount of insulin expenditure increases, Δ decreases and vice-versa. The ReMF and the ReME therapies can also be compared in Fig. 2E. The ReMF Pareto front dominates the ReME one (both Δ and ϕ_I are lower on the blue curve ($p = 1$) compared to the magenta curve ($p = 2$)). This indicates that a shot of insulin (the optimal solution of a ReMF problem is typically a pulsatile function) performs slightly better in terms of Δ than a therapy in which the drug is delivered over a longer period of time while using less insulin.

Figure 3 shows the results of the optimal control problem for the selected values of α_p and α_I . The blue and magenta curves are the optimal solutions of the ReMF and of the ReME problem, respectively. The orange curve corresponds to the case that 10 U of insulin are injected 30 minutes before the time of the meal, *i.e.*, , the standard therapy.

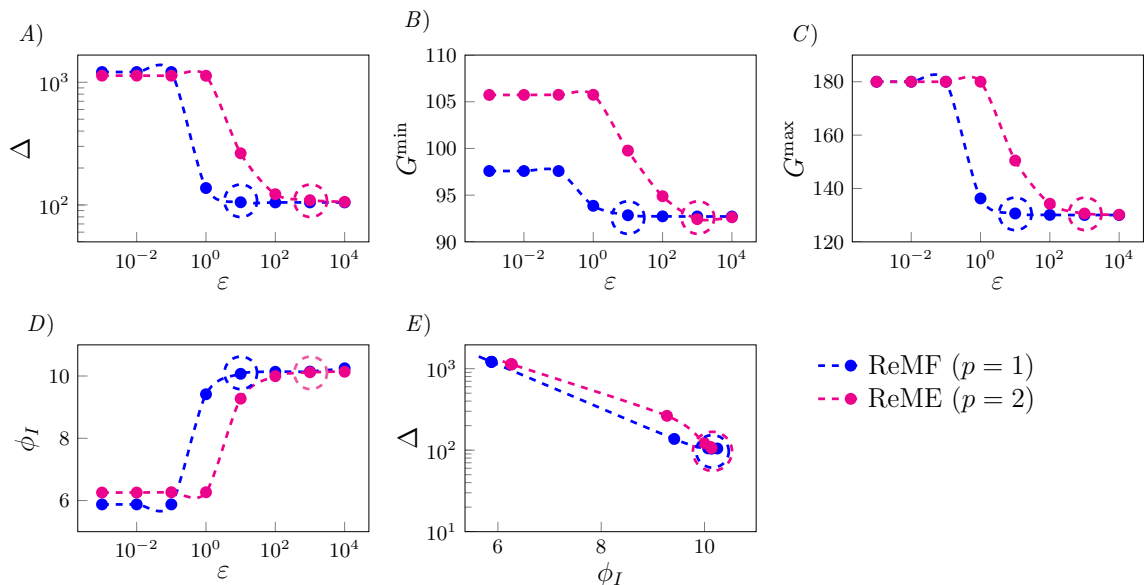


Fig 2. Performance of the optimal control solution as a function of ε . Large (small) values of ε correspond to a large (small) weight associated with the *BGI* index in the objective function, compared to the weight for insulin expenditure. The first four plots show our metrics as functions of the objective function coefficients: A) Δ vs. ε , B) G^{\min} vs. ε , C) G^{\max} vs. ε , and D) ϕ_I vs. ε . E) We also project the Pareto front into the $\Delta - \phi_I$ plane. We see a clear trade-off between Δ and ϕ_I as we vary ε . By increasing ε we can decrease the values of Δ and G^{\max} . However, the values of Δ and G^{\max} do not further decrease for ε larger than 10 for the ReMF problem ($p = 1$) and the value of Δ does not further decrease for ε larger than 10^3 for the ReME problem ($p = 2$). We choose $\varepsilon = 10$ for $p = 1$ and $\varepsilon = 10^3$ for $p = 2$, which are indicated by dashed circles in the figure, for the remaining simulations.

We observe that for $p = 1$ the optimal insulin infusion rate is pulsatile with a pulse appearing at $t \sim 20$ minutes, which is 40 minutes before the time of the meal. We obtained qualitatively similar results for different choices of the model parameters, with the pulse typically appearing at a time in the interval $t \in [20, 30]$ minutes. It is noteworthy that the optimal solution is close to the standard insulin based therapy for glucose regulation in diabetics. The optimal insulin infusion rate is continuous when we solve the ReME problem, also shown in the inset of Fig. 3B. Note that the ReMF and ReME therapies perform very similarly with respect to glucose as the peak insulin infusion rate occurs at approximately the same time and the total amount of insulin administered is nearly equal.

3.2 Insulin and Glucagon as Control Inputs

In the previous section we tuned the weights α_p and α_I inside the objective function (2). We now consider the case that $u_G > 0$ and we tune α_G , the weight associated with the glucagon expenditure in the objective function (2), by keeping $\alpha_p = 10$, $\alpha_I = 1$ for $p = 1$ and $\alpha_p = 10^3$, $\alpha_I = 1$ for $p = 2$, as previously determined.

In Fig. 4A, 4B and 4C, we plot the optimal Δ , G^{\min} and G^{\max} as functions of the parameter α_G , respectively. A large value of α_G indicates that we are placing a large weight on the expenditure of glucagon within the objective function (2), *i.e.*, the larger the value of α_G , the less glucagon we use. By looking at Fig. 4A, we observe that the values of Δ decrease as α_G decreases, *i.e.*, we can obtain lower (improved) values of Δ if we allow for a larger expenditure of glucagon. We note that past a certain value of α_G (10^{-2} in the both the ReMF and ReME problems) no further reduction in Δ is observed. As in the previous case, the maximum glucose level G^{\max} , shown in Fig. 4C, improves (decreases) when Δ improves (decreases). Interestingly,

different from the previous case, also the minimum glucose level G^{\min} (Fig. 4C) improves (increases) with Δ and G^{\max} : this is a consequence of the fact that we are using both insulin and glucagon as control inputs, which enables us to avoid both hypoglycemia and hyperglycemia.

In Fig. 4D we plot the projection of the Pareto front in the (ϕ_I, ϕ_G) plane. By looking at the figure, ϕ_I and ϕ_G appear to be positively correlated and related by an approximately linear relation. While the timing of administration of insulin and glucagon is different, we see that overall the more insulin is used in the optimal solution, the more glucagon is used as well. This is because the two hormones have opposite effects in the regulation problem and thus they work so as to balance each other. This is also consistent with the observation that with the dual drug therapy (insulin and glucagon) it becomes possible to simultaneously improve Δ , G^{\min} , and G^{\max} . From the data in Fig. 4D we derive the following approximate linear relationship between ϕ_G and ϕ_I ,

$$\phi_G(\phi_I) = 0.1596\phi_I - 1.5796 \quad (11)$$

Obviously, glucagon should be used only when $\phi_G(\phi_I) > 0$.

Panel 4E shows a projection of the Pareto front on the (ϕ_G, Δ) plane. We see again that the ReMF front dominates the ReME one, *i.e.*, a pulsatile therapy gives better results than a continuous therapy in terms of Δ and also uses lower amounts of the two drugs (smaller ϕ_G , and thus smaller ϕ_I due to the positive correlation found in Fig. 4D).

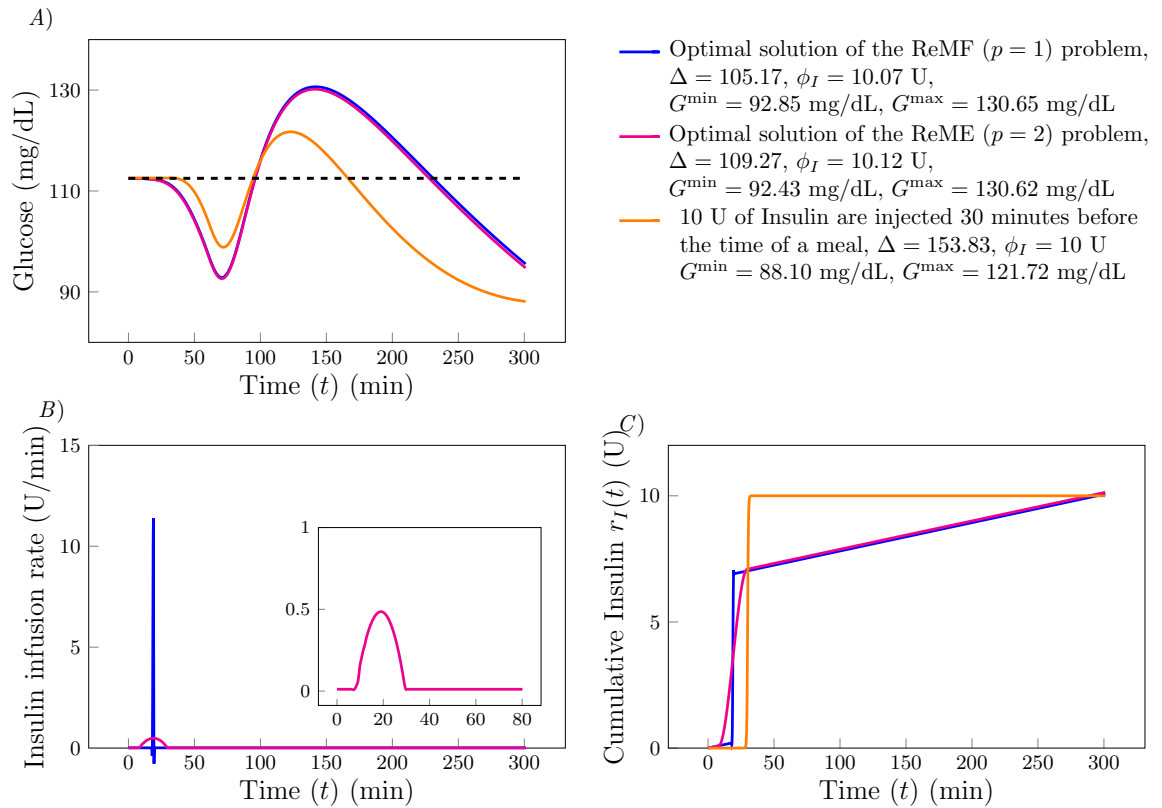


Fig 3. A) The time evolution of glucose $G(t)$ (in mg/dL). The blue curve corresponds to the pulsatile optimal insulin supply rate $u_I(t)$ (shown in B) obtained by solving the ReMF problem. The magenta curve corresponds to the continuous optimal insulin supply rate $u_I(t)$ (shown in B) obtained by solving the ReME problem. The orange curve is the time evolution of $G(t)$ corresponding to the standard therapy (10 U of insulin injected 30 minutes before the time of the meal). B) Time evolution of the optimal insulin infusion rates $u_I(t)$ (in U/min). Color code is consistent with A. C) Cumulative insulin supply $r_I(t)$ (in U) as a function of t .

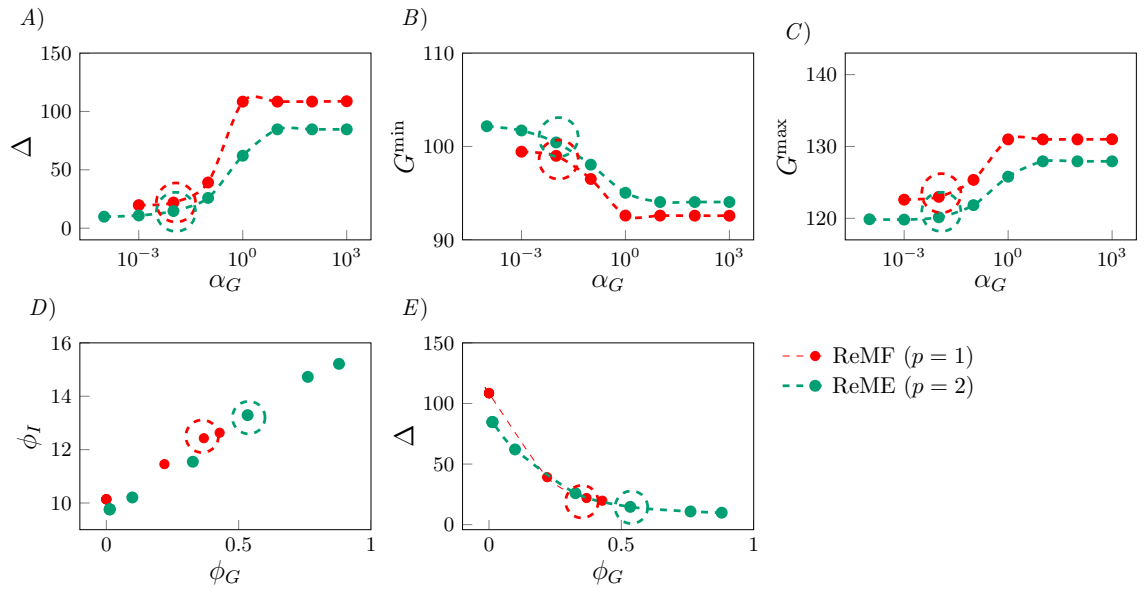


Fig 4. Performance of the optimal control solution as a function of α_G . A) Δ vs. α_G . B) G_{\min} vs. α_G . C) G_{\max} vs. α_G . D) ϕ_I vs. ϕ_G . E) Δ vs. ϕ_G . We select $\alpha_G = 10^{-2}$ for both of the ReMF and ReME problems, which are indicated by dashed circles in the figure.

The Pareto front is monotonically decreasing in Fig. 4E which indicates a trade-off between the total amount of drugs used and the achievable glucose control performance. We choose the value of α_G for which the ratio between the increase in Δ and the decrease in ϕ_G is minimized, *i.e.*, $\alpha_G = 10^{-2}$ for both ReMF and ReME problems, which are indicated by dashed circles in the figure.

Figures 5A and 5B show the results of the optimal control problem for $\alpha_p = 10$, $\alpha_I = 1$ and $\alpha_G = 10^{-2}$ when $p = 1$; and $\alpha_p = 10^3$, $\alpha_I = 1$ and $\alpha_G = 10^{-2}$ when $p = 2$. In Fig. 5A we plot the time evolution of glucose $G(t)$ for the different optimal solutions. The blue curve corresponds to the solution of the ReMF problem when only insulin is used (the blue curve in Fig. 3A). The red and green curves correspond to the solution of the ReMF and the ReME problems for the dual drug therapy. We observe that $G(t)$ reaches the desired level G_d faster if we use both insulin and glucagon as control inputs, compared to the case that only insulin is used. We also see that in this case both G^{\max} decreases and G^{\min} increases. We therefore conclude that the therapy with both insulin and glucagon performs better than the therapy with only insulin, as the risks for both hypoglycemia and hyperglycemia are reduced and glucose fluctuations are suppressed.

In Fig. 5B we plot the optimal insulin infusion rates and in Fig. 5C we plot the cumulative insulin supply $r_I(t)$ as a function of time t . We observe that for the ReMF problem, the pulse in insulin appears at $t = 32$ minutes in the case that both insulin and glucagon are used (28 minutes before the meal), whereas the pulse appears at $t = 20$ minutes when only insulin is used. From Fig. 5D, we see that, for the ReMF problem, the glucagon delivery function is pulsatile with a main pulse appearing at $t = 145$ min (one hour and 25 minutes after the meal) and a secondary pulse appearing at $t = 203$. The dual drug therapy shows a noticeable difference between the ReMF solution and the ReME solution. As expected, the solutions of the ReME problem are continuous. The glucose response to the ReME therapy is better than the glucose response to the ReMF solution. Specifically, the green curve has smaller oscillations (in panel A) at the cost of small increases in the total amounts of used insulin and glucagon (compare panels C and E).

Based on the results in Fig. 5, we propose a possible *ad-hoc* dual drug therapy to be used as an alternative to the standard therapy. Rather than administering insulin half an hour before the

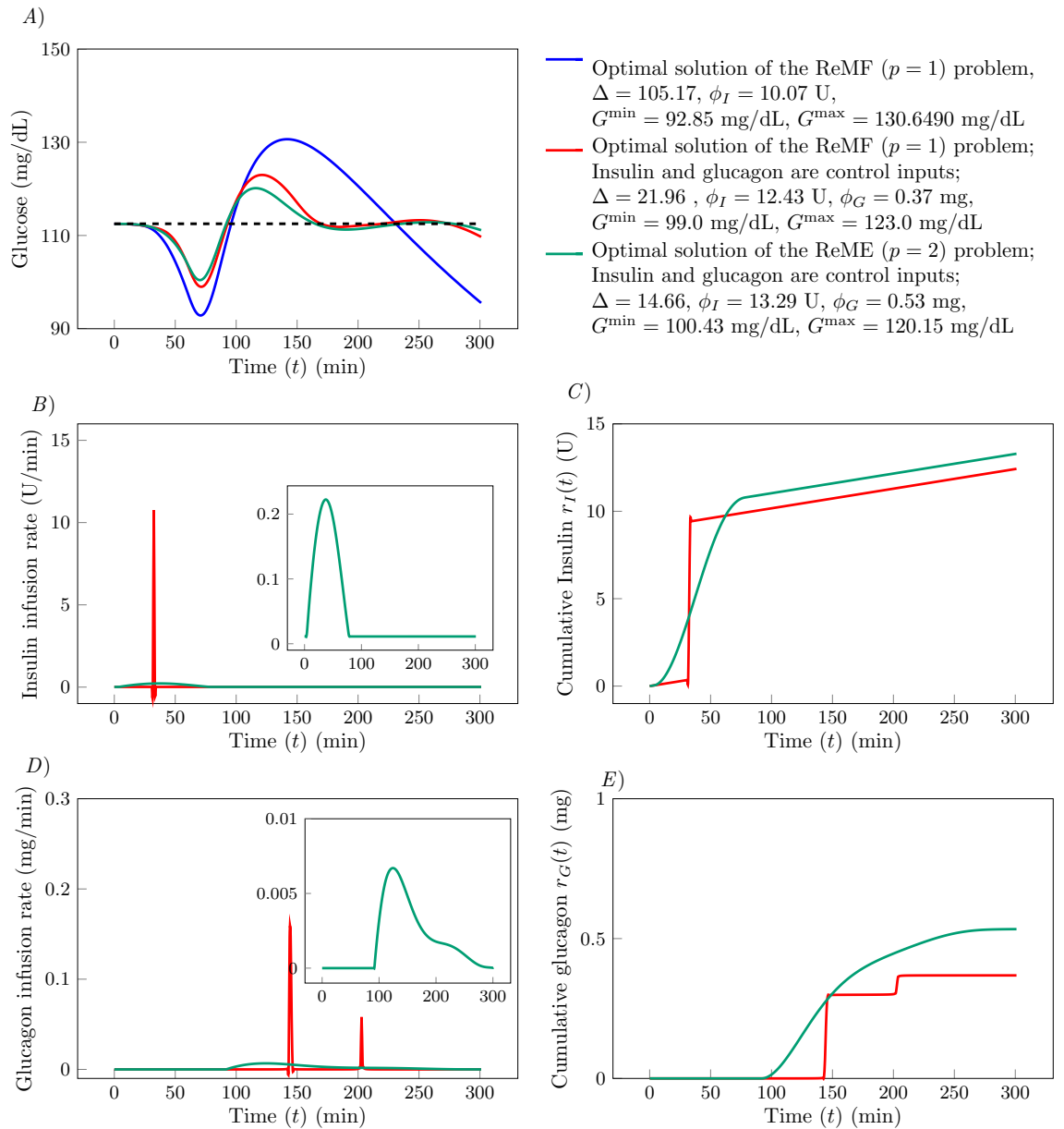


Fig 5. A) Time evolution of glucose $G(t)$ (in mg/dL). The blue curve corresponds to $u_I(t)$ obtained by solving the ReMF problem. The red curve corresponds to $u_I(t)$ and $u_G(t)$ obtained by solving the ReMF problem using the dual drug therapy. The green curve corresponds to $u_I(t)$ and $u_G(t)$ obtained by solving the ReME problem using the two-drug-therapy. B) Time evolution of the insulin infusion rate $u_I(t)$ (in mg/dL). Color code is consistent with A. C) The cumulative insulin supply $r_I(t)$ as a function of time t . D) Time evolution of the glucagon infusion rate $u_G(t)$ (in mg/dL). E) The cumulative glucagon supply $r_G(t)$ as a function of time t .

meal (standard therapy), better glucose regulation can be achieved with a slightly larger insulin injection half an hour before a meal followed by a glucagon injection one hour and thirty minutes after a meal. The insulin injection of the *ad-hoc* dual drug therapy is 25% larger than the one used in the standard therapy, which is consistent with the relation between ϕ_I for the monotherapy ReMF optimal solution and the one used in the dual drug therapy.

In Fig. 6 we present a comparison between the glucose response to the standard insulin base

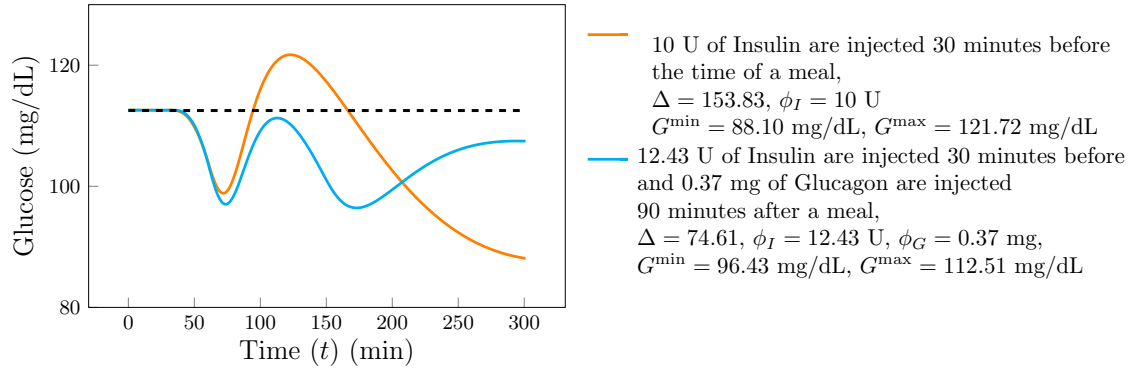


Fig 6. Comparison between the glucose response to the standard insulin base therapy (orange curve) and the proposed *ad-hoc* dual therapy (cyan curve).

therapy (orange curve) and the proposed *ad-hoc* dual therapy (cyan curve) for the case of a meal with 70 grams of glucose (for the particular patient considered this corresponds to 10 units of insulin half an hour before the meal) and the proposed *ad-hoc* dual drug therapy (which consists of 12.43 units of insulin thirty minutes before the meal and 0.40 mg of glucagon one hour and thirty minutes after the meal). We observe that the *ad-hoc* dual drug therapy performs better in terms of all of the proposed measures (Δ , G^{\min} , G^{\max} , ϕ_I and ϕ_G) as opposed to the standard insulin based therapy.

3.3 Robustness Analysis

We now analyze the robustness of the optimal control therapies we have proposed with respect to model parameter mismatches, which is a fundamental step for implementation of model based control. We consider two different types of mismatches. The first type accounts for variability in the patient's behavior, in terms of both the time of the meal τ_D and the amount of glucose intake D . The second type accounts for deviations in the parameter estimation, as well as the temporal variability of the parameters that a patient may experience during the day [4].

3.3.1 Robustness Against Variability of the Meal Time and Glucose Intake

In this section we analyze the robustness of the optimal ReMF therapies (both monotherapy and dual therapy) with respect to the two “control” parameters the patient has. The first one is the variation in the meal time, $(\bar{\tau}_D - \tau_D)$ (min), where $\bar{\tau}_D$ is the time of a meal and τ_D is the time of a meal we assumed in order to compute the optimal therapies. The second one is the variation of glucose in the meal, $(\bar{D} - D)$, where \bar{D} is the glucose intake in a meal and D is the glucose intake we assumed to compute the optimal therapies. We consider variations in the meal time $\bar{\tau}_D$ in the interval [30, 90] min and variations of the glucose intake \bar{D} in the interval [40, 100] g.

The results of this study are illustrated in Fig. 7. Figure 7 provides a visual assessment of the quality of the optimal therapies in terms of the three proposed measures Δ , G^{\max} and G^{\min} (the over-bar stands for evaluation at the perturbed parameter values $(\bar{\tau}_D, \bar{D})$). The color in Fig. 7 varies according to the control performance from green (good) to red (dangerous). In the upper panels (A–C) we consider the optimal ReMF monotherapy, while in the lower panels (D–F) we consider the optimal ReMF dual therapy. Cross symbols indicate the application of the optimal control therapies under ideal condition, *i.e.*, when $\bar{\tau}_D = \tau_D$ and $\bar{D} = D$. The black curves labeled by 180, 90 and 70 in Figs. 7B, 7C, 7D, 7E are the curve level plots for $\bar{G}^{\max} = G^U$, $\bar{G}^{\min} = G^L$ and $\bar{G}^{\min} = 70$, respectively. The black curves labeled by 180 in Figs. 7B, and 7E, are the curve level plots for $\bar{G}^{\max} = G^U$.

We see from Figs. 7A and 7D that the optimal therapies for the ReMF problem (using only

insulin or both insulin and glucagon) are robust with respect to variations in the control parameters: $\bar{\Delta}$ remains well bounded in most of the considered parameter space. In particular we see from Figs. 7B and 7E that the proposed optimal therapies are robust against hyperglycemic events: for example, even if \bar{D} exceeds D by 50% and $\bar{\tau}_D$ exceeds τ_D by 30 minutes, the patient will not enter the hyperglycemic regime ($G^{\max} > 300$). Figures 7C and 7F reveal that the proposed therapies suffer from a certain lack of robustness with respect to hypoglycemic events ($G^{\min} < 70$), the most dangerous ones. The dangerous cases are, however, confined to extreme situations in which $\bar{D} < 0.5D$ and $\bar{\tau}_D = \tau_D + 30$ minutes. Figures 7C and 7F show also that the optimal therapy for the ReMF problem with both insulin and glucagon is more robust (larger green region and smaller yellow region) than the optimal therapy for ReMF problem with only insulin (smaller green region and larger yellow region): thus the use of glucagon alleviates the risk of severe, life-threatening hypoglycemia.

We obtain qualitatively similar results when performing the same analysis for the other therapies we proposed (the ReME therapies and the *ad-hoc* dual drug therapy).

3.3.2 Robustness to Parameter Mismatches

We consider perturbation of the model parameters up to 20% of their nominal values,

$$\bar{\Theta}_i = \Theta_i(1 + \varphi), \quad (12)$$

where φ is a random number from a normal distribution $\mathcal{N}(0, 0.067^2)$, Θ_i is a nominal parameter for a given patient with basal glucose level G_b and $\bar{\Theta}_i$ represents the associated

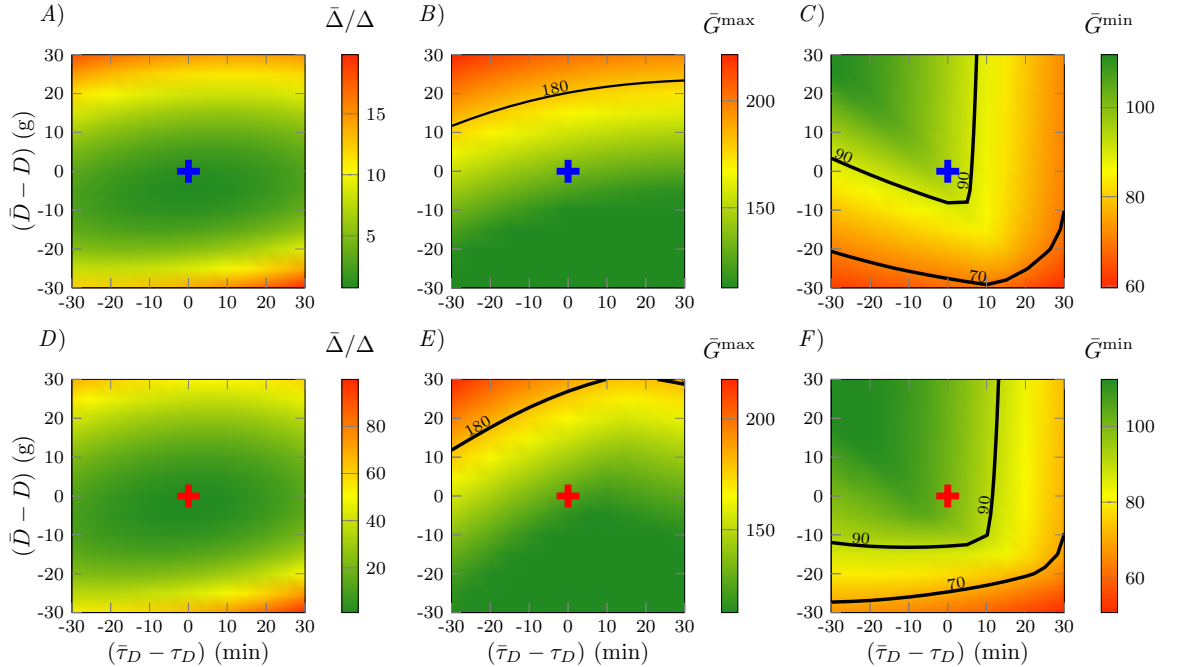


Fig 7. Robustness of the optimal control solution against variations in the meal timing and the amount of glucose in the meal. A)–C) show the results obtained for the ReNF problem ($p = 1$) with only insulin provided, D)–F) ReMF ($p = 1$) problem with both insulin and glucagon provided. Cross symbols indicate the application of the optimal control therapies for $\bar{D} = D$ and $\bar{\tau}_D = \tau_D$. The blue cross symbols correspond to the optimal therapies for the ReMF problem with only insulin. The red cross symbols correspond to the optimal therapies for the ReMF problem with both insulin and glucagon. A) and D) are plots of $\bar{\Delta}/\Delta$ in the control parameters space $(\bar{\tau}_D, \bar{D})$. B) and E) are the plots of \bar{G}^{\max} in the control parameters space $(\bar{\tau}_D, \bar{D})$. C) and F) are the plots of \bar{G}^{\min} in the control parameters space $(\bar{\tau}_D, \bar{D})$.

perturbed parameter. We then apply the optimal insulin and glucagon dosing, calculated for the unperturbed system, to 100 perturbed systems. This is analogous to testing the computed optimal control therapy on a specific patient, but the patient's parameters may vary due to imperfect knowledge or due to the parameter variability throughout the day. The results of this study are illustrated with a Control Variability Grid Analysis (CVGA), see Fig. 8. The CVGA provides a simultaneous visual and numerical assessment of the overall performance of the glycemic control strategies in terms of the achieved minimum/maximum glucose values in the space of parameters mismatches. In Fig. 8, points in the light green region indicate accurate blood glucose control while points in the dark green regions indicate the patient is not immediately at risk of either hypoglycemia or hyperglycemia. Points in the top two yellow/orange regions indicate an elevated risk of hyperglycemia and points in the the right two yellow/orange regions indicate an elevated risk of hypoglycemia. Finally, points in the red corner region indicate an elevated risk of both hyperglycemia and hypoglycemia. Each point reported in the figure is a plot of G^{\max} vs. G^{\min} . Here, the black dots correspond to the glucose response when a certain therapy is applied to a system with perturbed parameters. Cross symbols indicate application of the optimal control therapies to the unperturbed systems.

For the of monotherapy (ReMF in Fig. 8A and ReME in Fig. 8B) we find that the control is 67% and 61% accurate, respectively. For the dual therapy case (ReMF in Fig. 8C and ReME in Fig. 8D) we find the control is more accurate than for the case of monotherapy, 92% and 94%

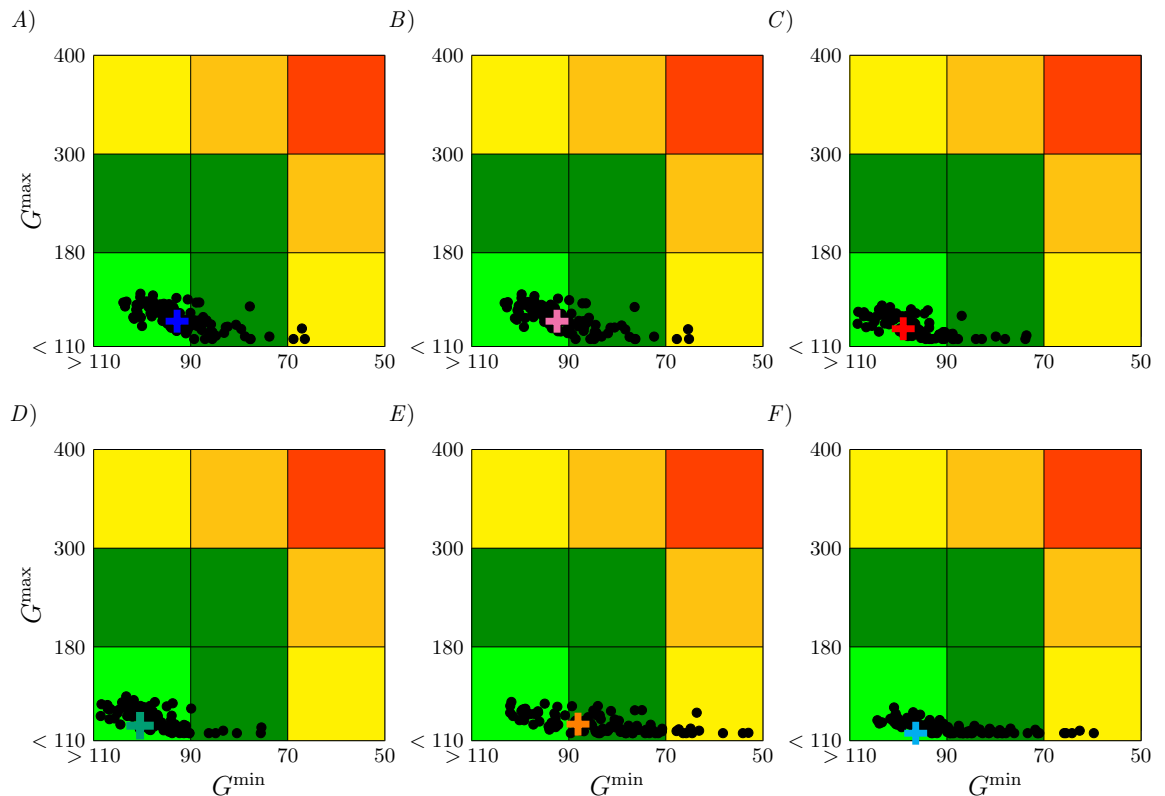


Fig 8. Robustness of the optimal control solution against parameter perturbations of the system and CVGA in the G^{\min} , G^{\max} plane. The analysis is performed for A) ReMF ($p = 1$) problem with only insulin provided, B) ReME ($p = 2$) problem with only insulin provided, C) ReMF ($p = 1$) problem with both insulin and glucagon provided, D) ReME ($p = 2$) problem with both insulin and glucagon provided, E) the standard therapy, and F) the proposed *ad-hoc* dual drug therapy. Cross symbols indicate the application of the optimal control therapies to the unperturbed systems.

accurate, respectively. The least robust control is obtained with the standard therapy (shown in Fig. 8E), attaining only 37% accuracy. Note that the optimal dual drug therapies (Figs. 8C and 8D) are not only more robust than the optimal insulin therapies (Figs. 8A and 8B), but also than the standard therapy (8E). We also see that the *ad hoc* therapy (8E) is more robust than the standard therapy (8E).

4 Discussion

In this paper we have used the Glucose-Insulin-Glucagon mathematical model proposed in [2–4], which describes how the body responds to exogenously supplied insulin and glucagon in patients affected by Type I diabetes and designed an optimal dosing schedule of either insulin or insulin and glucagon together to regulate the blood glucose index (BGI), while limiting the total amount of insulin and glucagon administered. The numerical optimal control software *PSOPT* has been used to solve this optimal control problem. While the numerical solution requires knowledge of the set of model parameters, which are patient specific, the solutions we obtain provide insight into the best possible glucose regulation with insulin or with insulin and glucagon together. Our approach is in agreement with the results of references [60–62], in which simplified models are used to analytically establish general theoretical properties and control limitations for the glucose regulation problem.

Two distinct regulation problems have been considered: the minimum fuel problem (ReMF) which yields pulsatile (shot-like) type solutions and the minimum energy problem (ReME) which yields longer periods of time over which insulin is administered but with smaller delivery rates. This has allowed us to compare standard therapies which typically consist in shots of insulin with therapies in which insulin is delivered continuously. In [63, 64] it has been proven that the optimal control is pulsatile when the aim of the control is to minimize the variation in the maximum and minimum output response, the system is positive (like the one we are considering) and the disturbance (the meal, in our case) is pulsatile. Our work indicates that pulsatile control is still a good choice when more complex objective functions are chosen. Moreover, a pulsatile control appears to be optimal for alternative more realistic models of the meal (for example, a meal that is consumed over a window of 15 minutes). We also see that a continuous drug delivery can achieve better results in the case of the dual therapy, thus pointing out the importance of developing a commercial pump able to deliver both insulin and glucagon.

For both the ReMF and ReME problems, we compute the optimal drug dosing schedules when only insulin is available and when both insulin and glucagon are available. The solution of the insulin only ReMF problem, astoundingly, is nearly equal to the standard method of insulin based glucose regulation. Similarly, the solution of the ReMF problem when insulin and glucagon are used is also pulsatile, except that the amount of insulin administered is larger and the administration time is closer to the time of the meal, while the glucagon is mostly delivered in a shot about an hour and thirty minutes after the meal.

The solution for the ReME problem when insulin only is available as well as when both insulin and glucagon are available is different from the ReMF solution in that, rather than being pulsatile, insulin and possibly glucagon are delivered at a slower rate over longer periods of time. Nonetheless, the total amount of insulin and possibly glucagon is about the same, and the peak of the longer delivery time occurs approximately at the same time of the shot according to the solution of the ReMF problem. The obtained glucose profiles for the optimal ReMF and ReME problem solutions do not differ too much from each other: taken together, these results indicate that the amounts of insulin and glucagon, and the peak times of delivery, are the most important factors to determine when computing the optimal solutions.

Based on the above results, we have proposed the following *ad hoc* therapy when insulin and glucagon are used in combination: *Administer a shot of insulin (with 5% more insulin than the amount required by the standard therapy based on the planned meal) 30 minutes before eating. Administer a shot of glucagon of an amount specified by Eq. (11) one hour and thirty minutes*

after completing the meal. This therapy must be used with caution as the amount of insulin injected can lead to hypoglycemia if the shot of glucagon is not administered as well.

All optimal dosing schedules we computed were tested for robustness with respect to variations in the meal timing and size and with respect to variability of the parameters. The therapies we proposed typically maintain the patient in the healthy region even under variable conditions and patient behavior. Note, however, that the proposed therapies are open-loop (the drug schedule is computed only from the condition of the patient at the initial time), thus cannot compensate for unexpected behavior that can arise due to modeling simplifications (*e.g.*, we do not consider how physical activity influences the blood glucose production and consumption [65, 66]), measurement noise or bias. A step towards the real application of our methodology is a real-time closed-loop strategy; this is possible, since the typical time needed to compute an optimal solution on a standard laptop (i7-8550U CPU with 16GB RAM) is around 2 minutes. Another main limitation of our study is that real life constraints and long term physiological effects may make a therapy based on exogenous administration of both insulin and glucagon impractical.

Our optimal control strategies require knowledge of the meal time and meal glucose amount. This is somewhat undesirable, as recent advances in diabetes therapy have moved towards devices that do not require the user to provide information about the meals. Our results emphasize the importance of knowing when the meals will occur, and that new dosing schedules would benefit from some knowledge about the meals. This seems to indicate that it would be beneficial to provide the pump with the ability to interpret the patient's behavior.

References

1. Dalla Man C, Rizza RA, Cobelli C. Meal simulation model of the glucose-insulin system. *IEEE Transactions on biomedical engineering*. 2007;54(10):1740–1749.
2. Dalla Man C, Raimondo DM, Rizza RA, Cobelli C. GIM, simulation software of meal glucose—insulin model; 2007.
3. Man CD, Micheletto F, Lv D, Breton M, Kovatchev B, Cobelli C. The UVA/PADOVA type 1 diabetes simulator: new features. *Journal of diabetes science and technology*. 2014;8(1):26–34.
4. Visentin R, Campos-Náñez E, Schiavon M, Lv D, Vettoretti M, Breton M, et al. The UVA/Padova Type 1 Diabetes Simulator Goes From Single Meal to Single Day. *Journal of diabetes science and technology*. 2018;12(2):273–281.
5. Steil GM, Rebrin K, Darwin C, Hariri F, Saad MF. Feasibility of automating insulin delivery for the treatment of type 1 diabetes. *Diabetes*. 2006;55(12):3344–3350.
6. Magni L, Raimondo DM, Man CD, Breton M, Patek S, De Nicolao G, et al. Evaluating the efficacy of closed-loop glucose regulation via control-variability grid analysis. *Journal of Diabetes Science and Technology*. 2008;2(4):630–635.
7. Magni L, Raimondo DM, Dalla Man C, De Nicolao G, Kovatchev B, Cobelli C. Model predictive control of glucose concentration in type I diabetic patients: An in silico trial. *Biomedical Signal Processing and Control*. 2009;4(4):338–346.
8. Palerm CC, Zisser H, Jovanovič L, Doyle III FJ. A run-to-run control strategy to adjust basal insulin infusion rates in type 1 diabetes. *Journal of process control*. 2008;18(3-4):258–265.
9. Bergenstal RM, Klonoff DC, Garg SK, Bode BW, Meredith M, Slover RH, et al. Threshold-based insulin-pump interruption for reduction of hypoglycemia. *New England Journal of Medicine*. 2013;369(3):224–232.

10. van Bon AC, Luijf YM, Koebrugge R, Koops R, Hoekstra JB, DeVries JH. Feasibility of a portable bihormonal closed-loop system to control glucose excursions at home under free-living conditions for 48 hours. *Diabetes technology & therapeutics*. 2014;16(3):131–136.
11. Nimri R, Muller I, Atlas E, Miller S, Fogel A, Bratina N, et al. MD-Logic overnight control for 6 weeks of home use in patients with type 1 diabetes: randomized crossover trial. *Diabetes Care*. 2014; p. DC_140835.
12. Capel I, Rigla M, García-Sáez G, Rodríguez-Herrero A, Pons B, Subías D, et al. Artificial pancreas using a personalized rule-based controller achieves overnight normoglycemia in patients with type 1 diabetes. *Diabetes technology & therapeutics*. 2014;16(3):172–179.
13. Mauseth R, Lord SM, Hirsch IB, Kircher RC, Matheson DP, Greenbaum CJ. Stress testing of an artificial pancreas system with pizza and exercise leads to improvements in the system's fuzzy logic controller. *Journal of diabetes science and technology*. 2015;9(6):1253–1259.
14. Reddy M, Herrero P, El Sharkawy M, Pesl P, Jugnee N, Thomson H, et al. Feasibility study of a bio-inspired artificial pancreas in adults with type 1 diabetes. *Diabetes technology & therapeutics*. 2014;16(9):550–557.
15. Parker RS, Doyle FJ, Peppas NA. A model-based algorithm for blood glucose control in type I diabetic patients. *IEEE Transactions on biomedical engineering*. 1999;46(2):148–157.
16. Parker RS, Doyle FJ, Peppas NA. The intravenous route to blood glucose control. *IEEE Engineering in Medicine and Biology Magazine*. 2001;20(1):65–73.
17. Gillis R, Palerm CC, Zisser H, Jovanovic L, Seborg DE, Doyle III FJ. Glucose estimation and prediction through meal responses using ambulatory subject data for advisory mode model predictive control; 2007.
18. Lynch SM, Bequette BW. Estimation-based model predictive control of blood glucose in type I diabetics: a simulation study. In: *Bioengineering Conference, 2001. Proceedings of the IEEE 27th Annual Northeast*. IEEE; 2001. p. 79–80.
19. Bruttomesso D, Farret A, Costa S, Marescotti MC, Vettore M, Avogaro A, et al.. Closed-loop artificial pancreas using subcutaneous glucose sensing and insulin delivery and a model predictive control algorithm: preliminary studies in Padova and Montpellier; 2009.
20. Marchetti G, Barolo M, Jovanovic L, Zisser H, Seborg DE. An improved PID switching control strategy for type 1 diabetes. *IEEE transactions on biomedical engineering*. 2008;55(3):857–865.
21. Fisher ME. A semiclosed-loop algorithm for the control of blood glucose levels in diabetics. *IEEE transactions on biomedical engineering*. 1991;38(1):57–61.
22. Bergman RN, Ider YZ, Bowden CR, Cobelli C. Quantitative estimation of insulin sensitivity. *American Journal of Physiology-Endocrinology And Metabolism*. 1979;236(6):E667.
23. Bergman RN, Phillips LS, Cobelli C. Physiologic evaluation of factors controlling glucose tolerance in man: measurement of insulin sensitivity and beta-cell glucose sensitivity from the response to intravenous glucose. *The Journal of clinical investigation*. 1981;68(6):1456–1467.

24. Bergman RN, Finegood DT, Ader M. Assessment of insulin sensitivity in vivo. *Endocrine reviews*. 1985;6(1):45–86.
25. Thabit H, Tauschmann M, Allen JM, Leelarathna L, Hartnell S, Wilinska ME, et al. Home use of an artificial beta cell in type 1 diabetes. *New England Journal of Medicine*. 2015;373(22):2129–2140.
26. Zavitsanou S, Mantalaris A, Georgiadis MC, Pistikopoulos EN. In Silico Closed-Loop Control Validation Studies for Optimal Insulin Delivery in Type 1 Diabetes. *IEEE Trans Biomed Engineering*. 2015;62(10):2369–2378.
27. Hovorka R, Canonico V, Chassin LJ, Haueter U, Massi-Benedetti M, Federici MO, et al. Nonlinear model predictive control of glucose concentration in subjects with type 1 diabetes. *Physiological measurement*. 2004;25(4):905.
28. Bequette BW. Challenges and recent progress in the development of a closed-loop artificial pancreas. *Annual reviews in control*. 2012;36(2):255–266.
29. Copp DA, Gondhalekar R, Hespanha JP. Simultaneous model predictive control and moving horizon estimation for blood glucose regulation in type 1 diabetes. *Optimal Control Applications and Methods*. 2018;39(2):904–918.
30. McCrimmon RJ, Sherwin RS. Hypoglycemia in type 1 diabetes. *Diabetes*. 2010;59(10):2333–2339.
31. Castle JR, Engle JM, El Youssef J, Massoud RG, Yuen KC, Kagan R, et al. Novel use of glucagon in a closed-loop system for prevention of hypoglycemia in type 1 diabetes. *Diabetes care*. 2010;33(6):1282–1287.
32. Bátora V, Tárnik M, Murgaš J, Schmidt S, Nørgaard K, Poulsen NK, et al. The contribution of glucagon in an artificial pancreas for people with type 1 diabetes. In: *American Control Conference (ACC), 2015. IEEE; 2015. p. 5097–5102.*
33. El-Khatib FH, Jiang J, Damiano ER. Adaptive closed-loop control provides blood-glucose regulation using dual subcutaneous insulin and glucagon infusion in diabetic swine. *Journal of Diabetes Science and Technology*. 2007;1(2):181–192.
34. El-Khatib FH, Russell SJ, Nathan DM, Sutherlin RG, Damiano ER. A bihormonal closed-loop artificial pancreas for type 1 diabetes. *Science translational medicine*. 2010;2(27):27ra27–27ra27.
35. Russell SJ, El-Khatib FH, Nathan DM, Magyar KL, Jiang J, Damiano ER. Blood glucose control in type 1 diabetes with a bihormonal bionic endocrine pancreas. *Diabetes care*. 2012; p. DC_120071.
36. El-Khatib FH, Russell SJ, Magyar KL, Sinha M, McKeon K, Nathan DM, et al. Autonomous and continuous adaptation of a bihormonal bionic pancreas in adults and adolescents with type 1 diabetes. *The Journal of Clinical Endocrinology & Metabolism*. 2014;99(5):1701–1711.
37. Russell SJ, El-Khatib FH, Sinha M, Magyar KL, McKeon K, Goergen LG, et al. Outpatient glycaemic control with a bionic pancreas in type 1 diabetes. *New England Journal of Medicine*. 2014;371(4):313–325.
38. Russell SJ, Hillard MA, Balliro C, Magyar KL, Selagamsetty R, Sinha M, et al. Day and night glycaemic control with a bionic pancreas versus conventional insulin pump therapy in preadolescent children with type 1 diabetes: a randomised crossover trial. *The Lancet Diabetes & endocrinology*. 2016;4(3):233–243.

39. El-Khatib FH, Balliro C, Hillard MA, Magyar KL, Ekhlaspour L, Sinha M, et al. Home use of a bihormonal bionic pancreas versus insulin pump therapy in adults with type 1 diabetes: a multicentre randomised crossover trial. *The Lancet*. 2017;389(10067):369–380.
40. Herrero P, Bondia J, Oliver N, Georgiou P. A coordinated control strategy for insulin and glucagon delivery in type 1 diabetes. *Computer methods in biomechanics and biomedical engineering*. 2017;20(13):1474–1482.
41. Boiroux D, Bátorá V, Hagdrup M, Wendt SL, Poulsen NK, Madsen H, et al. Adaptive model predictive control for a dual-hormone artificial pancreas. *Journal of Process Control*. 2018;68:105–117.
42. Shirin A, Klickstein I, Feng S, Lin YT, Hlavacek WS, Sorrentino F. Prediction of Optimal Drug Schedules for Controlling Autophagy. Accepted for publication in *Scientific Reports*. 2019;doi:10.1038/s41598-019-38763-9.
43. Shirin A, Klickstein IS, Sorrentino F. Optimal control of complex networks: Balancing accuracy and energy of the control action. *Chaos: An Interdisciplinary Journal of Nonlinear Science*. 2017;27(4):041103.
44. Kovatchev BP, Cox DJ, Gonder-Frederick LA, Clarke W. Symmetrization of the blood glucose measurement scale and its applications. *Diabetes Care*. 1997;20(11):1655–1658.
45. Kovatchev BP, Clarke WL, Breton M, Brayman K, McCall A. Quantifying temporal glucose variability in diabetes via continuous glucose monitoring: mathematical methods and clinical application. *Diabetes technology & therapeutics*. 2005;7(6):849–862.
46. Control D, Group CTR. The effect of intensive treatment of diabetes on the development and progression of long-term complications in insulin-dependent diabetes mellitus. *New England journal of medicine*. 1993;329(14):977–986.
47. Kirk DE. *Optimal control theory: an introduction*. Courier Corporation; 2012.
48. Chachuat B. *Nonlinear and dynamic optimization: From theory to practice*; 2007.
49. JDRF website: <http://www.jdrf.org>; 2018.
50. Klickstein I, Shirin A, Sorrentino F. Energy scaling of targeted optimal control of complex networks. *Nature communications*. 2017;8:15145.
51. Rao AV. A survey of numerical methods for optimal control. *Advances in the Astronautical Sciences*. 2009;135(1):497–528.
52. Ross IM, Karpenko M. A review of pseudospectral optimal control: From theory to flight. *Annual Reviews in Control*. 2012;36(2):182–197.
53. Becerra VM. Solving complex optimal control problems at no cost with PSOPT. In: *Computer-Aided Control System Design (CACSD), 2010 IEEE International Symposium on*. IEEE; 2010. p. 1391–1396.
54. Nocedal J, Wright S. *Numerical optimization*. Springer, New York, USA, 2006. 2006;.
55. Wächter A, Biegler LT. On the implementation of an interior-point filter line-search algorithm for large-scale nonlinear programming. *Mathematical programming*. 2006;106(1):25–57.

56. Russell-Jones D, Gall MA, Niemeyer M, Diamant M, Del Prato S. Insulin degludec results in lower rates of nocturnal hypoglycaemia and fasting plasma glucose vs. insulin glargine: a meta-analysis of seven clinical trials. *Nutrition, Metabolism and Cardiovascular Diseases*. 2015;25(10):898–905.
57. MiniMed 670G System User Guide website: <https://www.medtronicdiabetes.com/sites/user-guides/MiniMed/>; 2018.
58. Lorenzi M, Bohannon N, Tsalikian E, Karam JH. Duration of type I diabetes affects glucagon and glucose responses to insulin-induced hypoglycemia. *Western Journal of Medicine*. 1984;141(4):467.
59. Cox DJ, Kovatchev BP, Julian DM, Gonder-Frederick LA, Polonsky WH, Schlundt DG, et al. Frequency of severe hypoglycemia in insulin-dependent diabetes mellitus can be predicted from self-monitoring blood glucose data. *The Journal of Clinical Endocrinology & Metabolism*. 1994;79(6):1659–1662.
60. Townsend C, Seron MM, Goodwin GC. Characterisation of optimal responses to pulse inputs in the Bergman minimal model. *IFAC-PapersOnLine*. 2017;50(1):15163–15168.
61. Townsend C, Seron MM, Goodwin GC, King BR. Control Limitations in Models of T1DM and the Robustness of Optimal Insulin Delivery. *Journal of diabetes science and technology*. 2018;12(5):926–936.
62. Townsend C, Seron MM. Optimality of unconstrained pulse inputs to the Bergman minimal model. *IEEE Control Systems Letters*. 2018;2(1):79–84.
63. Goodwin GC, Mediolli AM, Carrasco DS, King BR, Fu Y. A fundamental control limitation for linear positive systems with application to Type 1 diabetes treatment. *Automatica*. 2015;55:73–77.
64. Goodwin GC, Carrasco DS, Seron MM, Mediolli AM. A fundamental control performance limit for a class of positive nonlinear systems. *Automatica*. 2018;95:14–22.
65. Hajizadeh I, Rashid M, Turksoy K, Samadi S, Feng J, Sevil M, et al. Incorporating Unannounced Meals and Exercise in Adaptive Learning of Personalized Models for Multivariable Artificial Pancreas Systems. *Journal of diabetes science and technology*. 2018;12(5):953–966.
66. Beneyto A, Bertachi A, Bondia J, Vehi J. A New Blood Glucose Control Scheme for Unannounced Exercise in Type 1 Diabetic Subjects. *IEEE Transactions on Control Systems Technology*. 2018;.
67. Man CD. Parameters; 2018. private communication by email.
68. The Epsilon Group; 2018. Available from <https://tegvirginia.com/software/tldms/>.
69. The implementation of the UVA/Pavoda model (1014) in this paper; 2019. Available from https://github.com/iklick/dallaman_2014.
70. Liu YY, Slotine JJ, Barabási AL. Controllability of complex networks. *Nature*. 2011;473(7346):167–173.
71. Ruths J, Ruths D. Control profiles of complex networks. *Science*. 2014;343(6177):1373 – 1376.
72. Summers TH, Lygeros J. Optimal sensor and actuator placement in complex dynamical networks. *IFAC Proceedings Volumes*. 2014;47(3):3784–3789.

73. Wang B, Gao L, Gao Y. Control range: a controllability-based index for node significance in directed networks. *Journal of Statistical Mechanics: Theory and Experiment*. 2012;2012(04):P04011.
74. Nepusz T, Vicsek T. Controlling edge dynamics in complex networks. *Nature Physics*. 2012;8(7):568–573.
75. Yuan Z, Zhao C, Di Z, Wang WX, Lai YC. Exact controllability of complex networks. *Nature communications*. 2013;4(2447).
76. Iudice FL, Garofalo F, Sorrentino F. Structural permeability of complex networks to control signals. *Nature communications*. 2015;6(8349).
77. Gao XD, Wang WX, Lai YC. Control efficacy of complex networks. *Scientific Reports*. 2016;6(28037).
78. Yan G, Tsekenis G, Barzel B, Slotine JJ, Liu YY, Barabási AL. Spectrum of controlling and observing complex networks. *Nature Physics*. 2015;11(9):779–786.
79. Yan G, Ren J, Lai YC, Lai CH, Li B. Controlling complex networks: how much energy is needed? *Physical review letters*. 2012;108(21):218703.
80. Sorrentino F, di Bernardo M, Garofalo F, Chen G. Controllability of complex networks via pinning. *Physical Review E*. 2007;75:046103.
81. Gates AJ, Rocha LM. Control of complex networks requires both structure and dynamics. *Scientific reports*. 2016;6.
82. Cornelius SP, Kath WL, Motter AE. Realistic control of network dynamics. *Nature Communications*. 2013;4:1942. doi:10.1038/ncomms2939.
83. Wang LZ, Su RQ, Huang ZG, Wang X, Wang WX, Grebogi C, et al. A geometrical approach to control and controllability of nonlinear dynamical networks. *Nature Communications*. 2016;7:11323. doi:10.1038/ncomms11323.
84. Zañudo JGT, Yang G, Albert R. Structure-based control of complex networks with nonlinear dynamics. *Proceedings of the National Academy of Sciences*. 2017;114(28):7234–7239. doi:10.1073/pnas.1617387114.
85. Klickstein I, Shirin A, Sorrentino F. Locally Optimal Control of Complex Networks. *Physical Review Letters*. 2017;119(26):268301. doi:10.1103/PhysRevLett.119.268301.

Supplementary Information

S1 GIGM Model and Parameters

S1.1 Overview of GIGM Model with Type I Diabetics

We consider the model in [3,4] which is a system of nonlinear differential equations (ODEs). In all equations, t is the physical time (in min), all subscripts b denotes basal state, and all of the parameters are given in the table S1. The system of nonlinear differential equations are given below:

Glucose Subsystem:

$$\dot{G}_p(t) = EGP(t) + Ra(t) - U_{ii} - E(t) - k_1 G_p(t) + k_2 G_t(t), \quad G_p(0) = G_{pb} \quad (S1a)$$

$$\dot{G}_t(t) = -U_{id}(t) + k_1 G_p(t) - k_2 G_t(t), \quad G_t(0) = G_{tb} \quad (S1b)$$

$$G(t) = \frac{G_p}{V_G}, \quad G(0) = G_b \quad (S1c)$$

Here G_p (in mg/kg) is the mass of plasma glucose; G_t (in mg/kg) is the mass of tissue glucose; G (in mg/dL) is plasma glucose concentration and V_g (in dL/kg) is the distribution volume of glucose; EGP is the endogenous glucose production (in mg/kg/min); Ra (in mg/kg/min) is the rate of glucose appearance in plasma; U_{ii} (in mg/kg/min) and U_{id} (in mg/kg/min) are insulin-independent and insulin-dependent glucose utilizations, respectively. Also k_1 and k_2 are the parameters.

Insulin Subsystem:

$$\dot{I}_p(t) = -(m_2 + m_4)I_p(t) + m_1 I_l(t) + R_{ia}(t), \quad I_p(0) = I_{pb} \quad (S2a)$$

$$\dot{I}_l(t) = -(m_1 + m_3)I_l(t) + m_2 I_p(t), \quad I_l(0) = I_{lb} \quad (S2b)$$

$$I(t) = \frac{I_p(t)}{V_I}, \quad I(0) = I_b \quad (S2c)$$

Here I_l (in pmol/kg) is the mass of liver insulin; I_p (in pmol/kg) is the mass of tissue insulin; I (in pmol/L) is the plasma insulin concentration; V_I (in L/kg) is the distribution volume of insulin; R_{ia} (in pmol/kg/min) is the rate of appearance of insulin in plasma; m_1, m_2, m_3 and m_4 are the parameters.

Glucose rate of appearance:

$$Q_{sto}(t) = Q_{sto1}(t) + Q_{sto2}(t), \quad G_{sto}(0) = 0 \quad (S3a)$$

$$\dot{Q}_{sto1}(t) = -k_{gri}Q_{sto1}(t) + D\delta(t - \tau_D), \quad Q_{sto1}(0) = 0 \quad (S3b)$$

$$\dot{Q}_{sto2}(t) = -k_{empt}(Q_{sto})(t)Q_{sto2}(t) + k_{gri}Q_{sto1}(t), \quad Q_{sto2}(0) = 0 \quad (S3c)$$

$$\dot{Q}_{gut}(t) = -k_{abs}Q_{gut}(t) + k_{empt}Q_{sto}(t)Q_{sto2}(t), \quad Q_{gut}(0) = 0 \quad (S3d)$$

$$Ra(t) = \frac{f \cdot k_{abs} \cdot Q_{gut}(t)}{BW}, \quad Ra(0) = 0 \quad (S3e)$$

$$k_{empt}(Q_{sto}) = k_{min} + \frac{k_{max} - k_{min}}{2} \quad (S3f)$$

$$\{\tanh[\alpha(Q_{sto} - b.D)] - \tanh[\beta(Q_{sto} - c.D)] + 2\} \quad (S3g)$$

Here Q_{sto} (in mg) is the amount of glucose in the stomach, Q_{sto1} (in mg) is the amount of liquid glucose in the stomach, Q_{sto2} (in mg) is the amount of solid glucose in the stomach, Q_{gut} (in mg) is the glucose mass in the intestine; D (in mg) is the amount of ingested glucose at time τ_D ; BW (in kg) is body weight; k_{empt} is the rate constant of the gastric emptying; $k_{gri}, k_{abs}, k_{max}, k_{min}, f, \alpha, \beta$ are the parameters.

Endogenous glucose production:

$$EGP(t) = k_{p1} - k_{p2}G_p(t) - k_{p3}X^L(t) + \xi X^H(t), \quad EGP(0) = EGP_b \quad (S4a)$$

$$\dot{I}'(t) = -k_i[I'(t) - I(t)], \quad I'(0) = I_b \quad (S4b)$$

$$\dot{X}^L(t) = -k_i[X^L(t) - I'(t)], \quad X^L(0) = I_b \quad (S4c)$$

$$\dot{X}^H(t) = -k_H X^H(t) + k_H \times \max[H(t) - H_b, 0], \quad X^H(0) = 0 \quad (S4d)$$

Here X^L (in) is delayed insulin action on EGP ; X^H is delayed glucagon action on EGP ; I' is delayed insulin in compartment 1; k_{p1} , k_{p2} , k_{p3} , ξ , k_i , k_H are the parameters.

Glucose utilization:

$$U_{ii}(t) = F_{cns} \quad (S5a)$$

$$U_{id}(t) = \frac{[V_{m0} + V_{mx} \cdot X(t)]G_t(t)}{K_{m0} + G_t(t)} \quad (S5b)$$

$$\dot{X}(t) = -p_{2U}X(t) + p_{2U}[I(t) - I_b], \quad X(0) = 0 \quad (S5c)$$

Here U_{ii} (in mg/kg/min) and U_{id} (in mg/kg/min) are insulin-independent and insulin-dependent glucose utilization; X (in pmol/L) is insulin in interstitial fluid; F_{cns} , V_{m0} , K_{m0} , p_{2U} are the parameters.

Renal excretion:

$$E(t) = \begin{cases} k_{e1}[G_p(t) - k_{e2}] & \text{if } G_p(t) > k_{e2} \\ 0 & \text{if } G_p(t) \leq k_{e2} \end{cases} \quad (S6)$$

Here $E(t)$ (in mg/kg/min) is the glucose renal exertion; k_{e1} is the parameter.

Glucagon kinetics and secretion:

$$\dot{H}(t) = -nH(t) + SR_H(t) + Ra_H(t), \quad H(0) = H_b \quad (S7a)$$

$$SR_H(t) = SR_H^s(t) + SR_H^d(t), \quad (S7b)$$

$$\dot{SR}_H^s(t) = -\rho \left[SR_H^s(t) - \max \left(\frac{\sigma[G_{th} - G(t)]}{\max(I(t) - I_{th}, 0) + 1} + SR_H^b, 0 \right) \right], \quad SR_H^s(0) = nH_b \quad (S7c)$$

$$SR_H^d(t) = \delta \max \left(-\frac{dG(t)}{dt}, 0 \right) \quad (S7d)$$

Here H (in ng/L) is the concentration of plasma glucagon; SR_H (in ng/L/min) is the glucagon secretion; Ra_H (in ng/L/min) is the rate of appearance of glucagon in plasma; SR_H^s (in ng/L/min) and SR_H^d (in ng/L/min) is the static and dynamic components of glucagon, respectively; n , ρ , I_{th} , δ are the parameters.

Subcutaneous insulin kinetics:

$$R_{ia}(t) = k_{a1}I_{sc1}(t) + k_{a2}I_{sc2}(t) \quad (S8a)$$

$$\dot{I}_{sc1}(t) = -(k_d + k_{a1})I_{sc1}(t) + IIR(t), \quad I_{sc1}(0) = I_{sc1ss} \quad (S8b)$$

$$\dot{I}_{sc2}(t) = k_d \cdot I_{sc1}(t) - k_{a2}I_{sc2}(t), \quad I_{sc2}(0) = I_{sc2ss} \quad (S8c)$$

$$IIR(t) = IIR_b + \frac{u_I(t)}{BW} \quad (S8d)$$

Here R_{ia} (in pmol/kg/min) is the rate of appearance of insulin in plasma; I_{sc1} (in pmol/kg) is the amount of nonmonomeric insulin in the subcutaneous space; I_{sc2} is the amount of

monomeric insulin in the subcutaneous space; $IIR(t)$ is the insulin infusion rate where IIR_b is the basal infusion rate (in pmol/kg/min) from body and u_I (in pmol/min) is the external insulin infusion rate; k_{a1}, k_{a2}, k_d are the parameters. As the exogenous insulin infusion rate appears in the above equation in pmol/kg/min, we divide u_I by the body weight BW in the equation. Note that here the u_I is in pmol/min. To convert the unit of insulin infusion rate u_I from U/min to pmol/min, we multiply u_I by 6944.4, that is the unit conversion is 1 U/min = 6944.4 pmol/min.

Subcutaneous glucagon kinetics:

$$\dot{H}_{sc1}(t) = -(k_{h1} + k_{h2})H_{sc1}(t) + GIR(t), \quad H_{sc1}(0) = H_{sc1ss} \quad (S9a)$$

$$\dot{H}_{sc2}(t) = k_{h1}H_{sc1}(t) - k_{h3}H_{sc2}(t), \quad H_{sc2}(0) = H_{sc2ss} \quad (S9b)$$

$$Ra_H(t) = k_{h3}H_{sc2}(t) \quad (S9c)$$

$$GIR(t) = GIR_b + \frac{u_G(t)}{BV} \quad (S9d)$$

Here H_{sc1} (in ng/L) and H_{sc2} (in ng/L) are the glucagon concentration in the subcutaneous space; IGR is the glucagon infusion rate where GIR_b is the basal glucagon infusion rate (in ng/L/min) from the body and u_I is the external glucagon infusion rate (in ng/min); k_{h1}, k_{h2}, k_{h3} are the parameters. As the exogenous glucagon infusion rate appears in the above equation in ng/L/min, we divide u_G by the body volume BV in the equation. Note that here the u_G is in ng/min. To convert the unit of glucagon infusion rate from mg/min to ng/min, we multiply u_G by 10^6 , that is the unit conversion is 1 mg/min = 10^6 ng/min.

We write the ODEs in Eqs. (S1)-(S9) in the form $\dot{\mathbf{x}}(t) = \mathbf{f}(\mathbf{x}(t), \mathbf{u}(t), \Theta_{G_b})$ where $\mathbf{x} \in \mathbb{R}^{17}$ and t is the physical time (in min). The variable x_1 represents G_p , the mass of glucose in plasma; the variable x_2 represents G_t , the mass of glucose in tissue; the variable x_3 represents the mass of liver insulin I_l ; the variable x_4 represents the mass of plasma insulin I_p ; the variable x_5 represents the amount of delayed insulin I' in compartment 1; the variable x_6 represents the amount of delayed insulin X^L action on EGP ; the variable x_7 represents the amount of solid glucose Q_{sto1} in the stomach; the variable x_8 represents the amount of liquid glucose Q_{sto2} in the stomach; the variable x_9 represents the glucose mass Q_{gut} in the intestine; the variable x_{10} represents the amount of interstitial fluid X ; the variable x_{11} represents the amount of static glucagon SR_H^s ; the variable x_{12} represents the amount of plasma glucagon H ; the variable x_{13} represents the amount of delayed glucagon X^H action on EGP ; the variable x_{14} represents the amount of nonmonomeric insulin I_{sc1} in the subcutaneous space; the variable x_{15} represents the amount of monomeric insulin I_{sc2} in the subcutaneous space; the variable x_{16} represents the amount of subcutaneous glucagon H_{sc1} in the subcutaneous space; the variable x_{17} represents the amount of subcutaneous glucagon H_{sc2} in the subcutaneous space. Also $\mathbf{u}(t) = [u_I(t) \quad u_G(t)]^T$, where u_I is the external insulin and u_G is the external glucagon. We define Θ_{G_b} as the set of parameters for which the basal glucose level is G_b .

S1.2 Parameters

There are a total of 46 parameters in Eqs. (S1)-(S9). The parameters are not given in [3]. We set all the parameters for ‘Glucose subsystem’, ‘Insulin subsystem’, ‘Glucose rate of appearance’, ‘Endogenous glucose production’, ‘Glucose utilization’, ‘Glucose utilization’, ‘Renal excretion’, ‘Subcutaneous insulin kinetics’ from the references [1, 2], except k_{p1}, V_{m0} and HE_b . According to [2], the parameters are chosen to satisfy the steady-state constraints in type I diabetes. The parameters k_{p1} and V_{m0} are set so that the steady state solutions provide the basal Glucose level G_b and $EGP_b = 2.4$. In Type I diabetes, the endogenous glucose production is high [2], so we choose $EGP_b = 2.4$ mg/kg/min. We set $IIR_b = 0$ and $GIR_b = 0$ as the model we consider is for Type I diabetes. The commercial version of the UVA/Pavoda simulator [68] allows computing blood glucose responses to supplied dosages of insulin for some patients, but does not provide all of the parameters. We tune the parameter HE_b so that the blood glucose response to insulin of the *patient* we consider in this paper is qualitatively similar to the blood

glucose response to insulin of a patient from the software [68] (adultaverage.mat). All of the parameters we use are listed in the Table S1 for reproducibility of the results. Our implementation of the model [3] has been published in GitHub [69].

The equations for k_{p1} and V_{m0} are given below:

$$k_{p1} = EGP_b + k_{p2}G_{pb} + k_{p3}I_b \quad (\text{S10a})$$

$$V_{m0} = \frac{(EGP_b - F_{cns})(K_{m0} + G_{tb})}{G_{tb}} \quad (\text{S10b})$$

The basal steady states are given below:

$$G_{pb} = G_b V_g \quad (\text{S11a})$$

$$G_{tb} = \frac{F_{cns} - EGP_b + k_1 G_{pb}}{k_2} \quad (\text{S11b})$$

$$I_{lb} = I_{pb} \cdot \frac{m_2}{m_1 + m_3} \quad (\text{S11c})$$

$$I_{pb} = \frac{IIR_b}{m_2 + m_4 - \frac{m_1 m_2}{m_1 + m_3}} \quad (\text{S11d})$$

$$I_{sc1ss} = \frac{IIR_b}{k_d + k_{a1}} \quad (\text{S11e})$$

$$I_{sc2ss} = \frac{k_d}{k_{a2}} I_{sc1ss} \quad (\text{S11f})$$

$$SR_{Hb}^s = nH_b \quad (\text{S11g})$$

$$H_{sc1ss} = \frac{GIR_b}{k_{h1} + k_{h2}} \quad (\text{S11h})$$

$$H_{sc2ss} = \frac{k_{h1}}{k_{h3}} H_{sc1ss} \quad (\text{S11i})$$

Here, the basal values G_b (in mg/dL), IIR_b (in pmol/kg/min) and GIR_b (in ng/L/min) are settable by the user.

S2 Network Representation of the GIGM Model

In this section we construct a *graph* representation of the GIGM model. A graph $\mathcal{G}(\mathcal{V}, \mathcal{E})$, consists of a set $\mathcal{V} = \{x_i\}, i = 1, \dots, n$ of nodes and a set \mathcal{E} of directed edges, where each edge is identified by an ordered pair $\{x_i, x_j\}$ of nodes $x_i, x_j \in \mathcal{V}$.

Complex networks typically consist of two parts; a set of nodes with their interconnections which represent the topology of the network, and the dynamics which describes the time evolution of the network nodes. The prescribed dynamics of the nodes can be linear or non-linear. We can construct a complex network from a dynamical system, simply by considering a state variable as a node and by drawing a directed edge from a node x_i to another node x_j if x_i appears in the time derivative of x_j . We call *driver nodes*, the nodes which directly connect to the external inputs. We call *target nodes*, the nodes which have prescribed state that must be satisfied at the final time [50].

A network representation of the GIGM model is shown in Fig. S1. Each one of the state variable $x_i, i = 1, \dots, 17$, in Eqs. (S1)-(S9) is associated with a node (shown as a green circle in the figure). A directed edge (shown as a black arrow in the figure) is drawn from node x_i to node x_j , if the state x_i appears in the time derivative of the state x_j . For instance, as G_t appears on the right hand side of Eq. (S1a), there exists an edge from node G_t to node G_p . In the model in Eqs. (S1)-(S9), u_I and u_G are the external inputs acting on the nodes I_{sc1} and H_{sc1} ,

Table S1. Average parameters

Parameter	Type I Value	Unit
BW	78 [1]	Kg
BV	78 [1]	L
V_g	1.49 [1]	dL/kg
k_1	0.065 [1,2]	min ⁻¹
k_2	0.079 [1,2]	min ⁻¹
V_I	0.04 [1]	L/kg
m_1	0.379 [1]	min ⁻¹
m_2	0.673 [1]	min ⁻¹
m_4	0.269 [1]	min ⁻¹
m_5	0.0526 [1]	min.kg/pmol
m_6	0.8118 [1]	dimensionless
HE_b	0.112 [1]	dimensionless
k_{p1}	change Eq. (S10)	mg/kg/min
k_{p2}	0.0021 [1,2]	min ⁻¹
k_{p3}	0.009 [1,2]	mg/kg/min per pmol/L
k_{p4}	0.0786 [1]	mg/kg/min per pmol/L
k_i	0.0066 [1]	min ⁻¹
k_{max}	0.0465 [1]	min ⁻¹
k_{min}	0.0076 [1]	min ⁻¹
k_{abs}	0.023 [1]	min ⁻¹
k_{gri}	0.0465 [1]	min ⁻¹
f	0.9 [1]	dimensionless
a	0.00016 [1]	mg ⁻¹
b	0.68 [1]	dimensionless
c	0.00023 [1]	mg ⁻¹
d	0.009 [1]	dimensionless
F_{cns}	1 [1]	mg/kg/min
V_{m0}	changes (Eq. (S10))	mg/kg/min
V_{mx}	0.034 [1]	mg/kg/min per pmol/L
K_{m0}	4661.21	mg/kg
P_{2u}	0.084 [1]	min ⁻¹
k_{e1}	0.0007 [1]	min ⁻¹
k_{e2}	269 [1]	mg/kg
k_d	0.0164 [2]	min ⁻¹
k_{a1}	0.0018 [2]	min ⁻¹
k_{a2}	0.0182 [2]	min ⁻¹
δ	0.682 [3]	(ng/L per mg/dL)
σ	1.093 [3]	min ⁻¹
n	0.15 [3]	min ⁻¹
ζ	0.009 [3]	(mg/kg/min per ng/L)
ρ	0.57 [3]	(ng/L/min per mg/dL)
k_H	0.16 [3]	min ⁻¹
I_{th}	I_b [3]	(pmol/L)
G_{th}	G_b [3]	mg/dL
k_{h1}	0.0164 [3]	min ⁻¹
k_{h2}	0.0018 [3]	min ⁻¹
k_{h3}	0.0182 [3]	min ⁻¹

Average parameters.

Table S2. Basal values

Basal	Type I Value	Unit
X_b^H	0 [67]	pmol/L
EGP_b	2.4 [2]	mg/kg/min
H_b	93 [67]	ng/L
IIR_b	0 [2]	pmol/kg/min

Basal values.

respectively. Thus the set of drivers node $\mathcal{D} = \{I_{sc1}, H_{sc1}\}$. In this model as the plasma glucose G_p is the only variable we are trying to affect through the control action, thus the set of target nodes $\mathcal{T} = \{G_p\}$. In the figure, the driver nodes are colored cyan and the target node are colored magenta. As can be seen, the effect of the control inputs on the target node is mediated by the network structure, thus this particular structure plays an important role in our ability to control the network output. While the effect of the network topology has been investigated in the case of linear network dynamics, see e.g. [70–81], the case of nonlinear networks has so far received only limited attention [82–85]. Reference [42] and this paper investigate this problem in the context of two applications of interest to the medical field.

S3 Continuous Approximation of Non-differential Function in ODEs

The optimization algorithms implemented in *PSOPT* require the derivatives of the function $\mathbf{f}(\mathbf{x}(t), \mathbf{u}(t), \Theta_{G_b})$ exists. We notice that there are discontinuities in Eqs. (S1)-(S9).

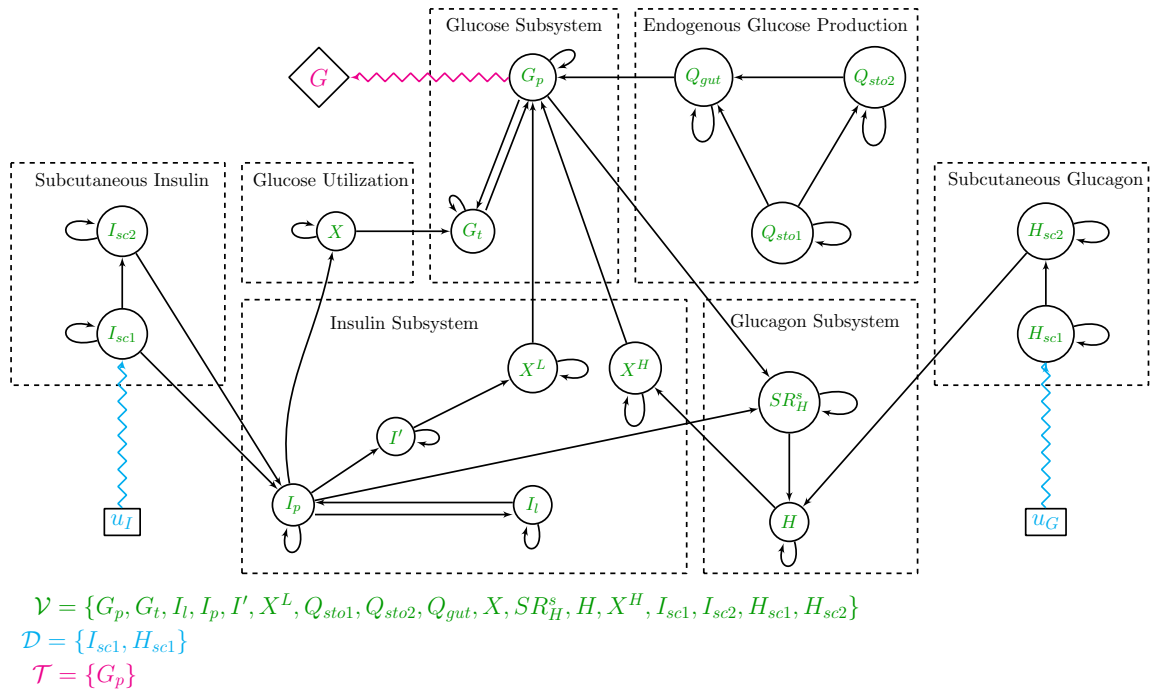


Fig S1. Network representation of the GIGM model.

The smooth approximation of the Renal exertion function $E(t)$ in Eq. (S6) by using a Heaviside function is,

$$E(t) = k_{e1}(G_p(t) - k_{e2}) \times \mathcal{H}(G_p(t), k_{e2}, k), \quad (\text{S12})$$

where,

$$\mathcal{H}(G_p(t), k_{e2}, k) = \frac{1}{1 + e^{-k(G_p - k_{e2})}}, k \in \mathbb{Z}. \quad (\text{S13})$$

Here a larger k corresponds to a sharper transition around $G_p(t) = k_{e2}$.

We define a continuous approximation of the Dirac delta function $\delta(t - \tau_D)$ in Eq. (S3c),

$$\delta(t - \tau_D) = \frac{d}{dt} \mathcal{H}(t, \tau_D, k), \quad (\text{S14})$$

where $\mathcal{H}(t, \tau_D, k) = \frac{1}{1 + e^{-k(t - \tau_D)}}$, $k \in \mathbb{Z}$. Here a larger k corresponds to a sharper transition at $t = \tau_D$.

We also define continuous approximation of the $\max(\cdot)$ function, e.g. in Eq. (S4d), as

$$\max(H(t) - H_b, 0) = (H(t) - H_b) \times \mathcal{H}(H(t), H_b, k), \quad (\text{S15})$$

where $\mathcal{H}(H(t), H_b, k) = \frac{1}{1 + e^{-k(H - H_b)}}$, $k \in \mathbb{Z}$. Here a larger k corresponds to a sharper transition at $H(t) = H_b$. In all our approximation we set $k = 4$.